Validation of the DRAGON/DONJON Code Package for MNR Using the IAEA 10 MW Benchmark Problem

S. E. Day and Wm. J. Garland
McMaster Nuclear Reactor
McMaster University
1280 Main St. W., Hamilton
Ontario, Canada L8S 4K1
Email: dayse@mcmaster.ca

Abstract

The first step in developing a framework for reactor physics analysis is to establish the appropriate and proven reactor physics codes. The chosen code package is tested, by executing a benchmark problem and comparing the results to the accepted standards. The IAEA 10 MW Benchmark problem[1] is suitable for static reactor physics calculations on plate-fueled research reactor systems and has been used previously to validate codes for the McMaster Nuclear Reactor[2] (MNR).

The flexible and advanced geometry capabilities of the DRAGON[3,4] transport theory code make it a desirable tool, and the accompanying DONJON[5,6] diffusion theory code also has useful features applicable to safety analysis work at MNR. This paper describes the methodology used to benchmark the DRAGON/DONJON code package against this problem and the results herein extend the domain of validation of this code package. The results are directly applicable to MNR and are relevant to a reduced-enrichment fuel program.

The DRAGON transport code models, used in this study, are based on the 1-D infinite slab approximation whereas the DONJON diffusion code models are defined in 3-D Cartesian geometry. The cores under consideration are composed of HEU (93% enrichment), MEU (45% enrichment) and LEU (20% enrichment) fuel and are examined in a fresh state, as well as at beginning-of-life (BOL) and end-of-life (EOL) exposures.

The required flux plots and flux-ratio plots are included, as are transport theory code k_∞ and diffusion theory code k_{eff} results. In addition to this, selected isotope atom densities are charted as a function of fuel burnup. Results from this analysis are compared to and are in good agreement with previously published results.

1.0 Introduction

The first step in developing a framework for reactor physics analysis is to establish the appropriate and proven reactor physics codes. The chosen code package is tested, by executing a benchmark problem and comparing the results to the accepted standards.

For plate-fueled research reactors a common benchmark problem is that outlined by the IAEA in IAEA-TECDOC-233[1]. This benchmark problem will herein be referred to as the IAEA 10 MW Benchmark Problem. It is not only appropriate for general plate-type fuel in research reactors but is also applicable for use in a reduced enrichment fuel program. The problem was specified at the

Consultants Meeting on "Preparation of a Programme on Research Reactor Core Conversions to Use LEU Instead of HEU", IAEA, June 19-22, 1979, in Vienna, Austria.

The IAEA 10 MW Benchmark problem consists of modelling three different enrichment cores (93%, 45% and 20% U-235 enrichment) in a fresh state as well as at both beginning-of-life (BOL) and end-of-life (EOL) exposures. The BOL to EOL stage constitutes a 5% U-235 depletion step. The problem is based upon a fictitious 10 MW_{th}, 6 x 5 element core with a central flux trap. The core is reflected by single graphite rows on two sides and is surrounded by light water. It possesses four-fold symmetry in the x-y plane and is also axially symmetric about a centerline. The core layout is shown in Figure 1. The fuel is plate-type with the standard and control assemblies containing 23 and 17 fuel plates respectively. Cross sectional views of the standard and control assemblies are shown in Figures 2 and 3.

Although the axial characteristics of the core are not specified in the body of IAEA-TECDOC-233, it has been extended by the ANL group in their modelling of the problem (Appendix F of Reference 1). The axial geometry used by the ANL group is adopted in this study. This extension is summarized below:

- The active height of the core is 60 cm, symmetric about an axial centerline.
- Above and below the active region of the core are 20%/80% by volume Aluminum/H_2O regions of 10 cm axial extent.
- Beyond the Aluminum/H_2O regions are light water regions 10 cm in axial extent.

This benchmark problem was used previously by MNR[2] to validate the WIMS-AECL/3DDT code package for work relating to the switch from 93% enriched HEU fuel to 20% enriched LEU fuel.

The flexible and advanced geometry capabilities of the DRAGON[3,4] transport code make it a desirable tool and the accompanying DONJON[5,6] diffusion code also has useful features applicable to safety analysis work at MNR. This benchmark extends the domain of validation of the DRAGON/DONJON code package and describes the methodology used to benchmark the code package against this problem. The results are directly applicable to MNR and are relevant to a reduced-enrichment fuel program.

2.0 Codes

The codes used in this analysis were developed and remain property of École Polytechnique de Montréal, Quebec, Canada.

Both codes used in this analysis are modular in design with respect to their calculational and data handling routines. The modules for the respective codes are linked together using the GAN generalized driver[3], which facilitates straightforward interfacing with other production codes.

The input files for each code are written in the CLE-2000 programming language[3], which allows for logical programming and thus for a more flexible input file structure than a typical sequential-record input.

2.1 DRAGON

DRAGON is a multi-group transport theory code. The main modules are the multigroup flux solver and the one-group collision probability (CP) tracking modules, which only differ in the level of approximation in the CP calculations.

The CP tracking modules allow for extensive geometry capabilities including 2-D and 3-D Cartesian modelling, which is an improvement over the allowable geometries for the WIMS-AECL[7] code. In the latter, plate-fuel modelling is restricted to a 1-D infinite slab approximation. Similarly, larger region WIMS-AECL modelling must be approximated by either: a 1-D infinite-slab model or a 2-D annular model.

The code also contains modules for isotopic depletion calculations and production of condensed and/or homogenized nuclear properties for reactor calculations.

The versions of the code and library used in this analysis are listed below:

- DRAGON Version 971124 (1997/11/24) also known as DRAGON 3.02
- WIMS-AECL ENDF/B-V-based library (HP 9000 1994 Nov 5)

The library is based on the ENDF/B-V data file, and contains cross sections for 145 nuclides, including 20 fissile isotopes and 45 fission products, in 89 energy groups. The energy group structure is divided into 42 thermal groups, 23 resonance groups and 24 fast groups.

The code was used to produce homogenized and condensed cross sections for the various regions of the core, which were then used in the diffusion theory core model. The companion diffusion theory code, DONJON, is described in Section 2.2.

2.2 DONJON

DONJON is a multi-group diffusion theory code capable of simulating both static and kinetic problems. Similar to standard diffusion codes the DONJON code solves the multi-dimensional, multi-group time-independent diffusion equation. Provisions for homogeneous, spherical, cylindrical, Cartesian and hexagonal geometry are available.

The version of DONJON used in this study is:

- DONJON version 980202 (1998/02/02) also known as DONJON 2.00

In addition to the static diffusion equation solution, DONJON also has kinetics capabilities for analyzing such scenarios as device movement or fuel burnup. Kinetics analysis is done using the improved quasi-static method.[8] This is based on flux factorization into an amplitude function, T, and a shape function, φ as:

$$\phi(\mathbf{r}, E, t) = T(t) * \varphi(\mathbf{r}, E, t)$$

T(t) is obtainable as a point kinetics solution while $\varphi(\mathbf{r},E,t)$ is the solution of a shape equation coupled with the point kinetics system.

This benchmark problem is for static core-model solutions only.

3.0 Methodology

The DRAGON transport theory code was used to produce homogenized few-group cross sections, which were subsequently used as input to the DONJON core models. This is a standard analysis technique.

The methodology used in this analysis was based on previous work performed on the IAEA 10 MW Benchmark Problem, which is summarized in Reference 1. The specifics of both the transport and diffusion theory models are discussed in the following 2 sections.

3.1 DRAGON Cell Models

In general, the transport theory part of reactor physics analysis is geared towards providing suitably averaged cross sections for small regions of the system under consideration. As diffusion theory analysis is not suitable for regions with strong absorption, it cannot be used for cell calculations because of the presence of the highly absorbing fuel regions even if it is valid at the level of reactor calculations with low absorption homogenized cell properties. The heterogeneous cell calculations must therefore be performed using a transport theory model. The transport theory model output included average (homogenized) cross sections, which are then used as input for a diffusion theory model of the entire system. A diffusion theory model is required as a transport theory solution is too expensive (in terms of memory and computer time) for a geometry on the scale of an entire core.

The accepted approach in the previously published IAEA 10 MW Benchmark studies revolves around a 1-D infinite slab approximation to the geometry for the plate-fuel. This is accepted largely because the individual fuel-plate (meat and clad) dimensions and the inter-plate (coolant gap) dimensions are small, relative to the width of the fuel plates (see Figures 2 and 3). In addition to this, the approximation is best suited to plate-fuel in which the material beyond the active width of the fuel (the clad and moderating material beyond the fuel meat and the support side-plates) is small in volume compared to the material within the active width of the fuel. The approximation in this model is the relocation of this “peripheral” material.

The dimension modelled in the 1-D infinite slab approximation is that in the direction of the thickness of the individual fuel plates, *i.e.*, perpendicular to the long face of the fuel plates. As such, the inter-plate dimensions are modelled explicitly.

Although DRAGON allows for explicit modelling of 2-D and 3-D Cartesian geometries the 1-D infinite slab geometry approximation was adopted for this study as that is what is currently being used for MNR models using the WIMS-AECL/3DDT code package.

Most of the work included in Reference 1 seems to be based on models representing one individual fuel plate and its appropriate environment. This environment includes the adjacent coolant gaps and a proportional amount of the structural material and surrounding moderator. An alternative approach to modelling a fuel assembly is to explicitly model all of the fuel plates, maintaining the actual inter-plate distances. The peripheral structural and moderating material is included as separate slab regions beyond the outer fuel plates. This latter approach tends to lend more information to the inter-plate relationships, and is herein referred to as a “multi-plate”

model, although both models may be considered appropriate in the 1-D approximation. The multi-plate fuel model was used for this analysis in the comparisons with previously published results.

A "half-plate" model can represent an individual fuel plate, with a reflective centerline in the central fuel region. Similarly only half of the assembly need be modelled with a reflective centerline condition for a multi-plate model of the standard and control fuel assemblies. Half-plate, one-plate and multi-plate models are shown in Figure 4 for standard fuel. The one-plate model serves as a check on the symmetry boundary condition used in the half-plate model, as the effective geometry should be identical.

Separate control-fuel models were constructed. It should be noted that in all of the previously published work the same fuel-plate transport theory model was used to produce cross sections for the standard fuel assemblies as well as the fuel-plate regions of the control fuel assemblies. The vacant absorber gaps in the control fuel assembly account for a larger amount of light water moderator in the vicinity of the fuel plates thus leading to a more thermal spectrum. It was felt that a separate model was more realistic.

Burnup dependent cross sections were generated based on average plate power. These cross sections were homogenized over the entire fuel and control-fuel assemblies.

A buckling of 7.838×10^{-3} cm^{-2} was provided as user input in the DRAGON fuel models. This is derived as the geometric buckling of a 60 cm cylinder of radius 22.72 cm with 8 cm reflector savings above, below and radially. The radius of 22.72 cm gives an area equal to that of the fuel and central flux trap of the IAEA 10 MW Benchmark core.

The non-fuel sections of the reactor core and reflector (graphite, water trap and light water reflector) were represented with the appropriate "homogeneous" models. This is a standard technique, which was adopted by some of the groups reporting in Reference 1. The homogeneous model incorporates a very dilute fission source, *i.e.*, 10^{-10} atoms/bcm of U-235. An alternative approach to this is to model a section of the core large enough to contain some fuel material and to select only the non-fuel region of interest for cross section generation. This more complicated approach was not adopted in this study.

The benchmark problem demands specific fuel burnups for the BOL and EOL cores, given in percent depletion of U-235. The DRAGON code performs fuel evolution calculations (EVO: module) based on a user input time-step (in days) and power rating (megawatts per tonne of initial heavy elements = MW/THE). The result is a cross section file incremented in MWd/THE. As a result it was required to find the relationship between MWd/THE and percentage U-235 depletion. This was achieved by examining the U-235 atom densities given in the ASCII DRAGON output for each specific burnup step. The calculated MWd/THE values, corresponding to the specific U-235 depletions, were then given as user input in the DONJON core models.

All calculations were performed in the full 89-group library energy group structure and were condensed to the 5-group structure shown in Table 2. The 5-group structure was used for the DONJON diffusion theory calculations. Flux and flux-ratio results are presented in the 3-group structure indicated in Reference 1. This 3-group structure is also shown in Table 2.

3.2 DONJON Core Models

The diffusion theory (core) models were constructed in 3-D Cartesian coordinates, the 2-D details of which are shown in Figure 1. Using symmetry these models explicitly represent $1/8^{th}$ of the core. As indicated in Figure 1, a three-fuel-element thickness of the surrounding water reflector was included. Zero flux boundary conditions were used on the outer radial reflector boundaries as indicated in Figure 1. A void boundary condition was used on the outer boundary in the axial direction. These axial characteristics were introduced by ANL in Appendix F of Reference 1.

The spatial mesh used in the core models is shown in Figures 5-7 for the X, Y and the Z-direction respectively. In summary, constant mesh spacing of 1.35 cm, 1.28 cm and 1.0 cm were adopted for the X, Y, and Z directions respectively. This leads to an overall spatial mesh of 36 x 39 x 60 for the $1/8^{th}$ core.

4.0 Results

The results of the benchmark calculations are summarized in this section. The benchmark problem requires flux plots and flux-ratio plots for the different fuel types at specific percent U-235 depletion. However, due to the different rate of burn of U-235 in the fuel types, this results in comparing fuel which has had much different lengths of exposure (the LEU fuel depletes much slower than the HEU fuel). Therefore it was decided to compare the fuel at equal MWd exposure as was done in the ANL-79[1] and MNR-98 studies.

In addition to the required flux and flux-ratio plots, the transport theory eigenvalues, k_{∞}, with respect to burnup, and specific fuel-meat isotope evolutions are tabulated for each fuel type. Diffusion theory eigenvalues, k_{eff}, are compared with previously published results, as are core reactivity changes with respect to fuel burnup and enrichment change.

4.1 Burnup Dependence of Isotope Atom Densities

Some specific isotopes in the fuel regions of the transport theory models were examined with respect to burnup. The data was extracted in the same manner that the U-235 atom densities were extracted from the DRAGON ASCII output, for use in the burnup determination for the DONJON models. Data was interpolated using cubic spline calculations, with the fine temporal spacing of burnup data assuring minimal error in the interpolated values. Interpolation was necessary to determine atom densities at the specific burnup stages.

Data for each isotope in each fuel type are shown in Tables 3-8 at burnup stages of 0-50% U-235 depletion in increments of 5%. Agreement with the results published in the ANL-79 study is reasonable with some discrepancies in the Pu, Xe-135 and Sm-149 buildup. This can probably be attributed to using different cross section libraries.

The isotope buildup and depletion chains are slightly different in the control fuel assemblies relative to the standard fuel assemblies. This is reflected in the U-238 depletion and Pu buildups in Tables 3-8 and indicates that separate models for these two assembly types are justified.

4.2 DRAGON Model Eigenvalues

The eigenvalues, k_{∞}, from the DRAGON cell models, are shown in Table 9 for the standard and control fuel. The k_{∞} values from the DRAGON models for the standard 23-plate fuel agree very well with the previously published results, which are shown in Figures 8-10.

For all three fuel enrichments, the k_{∞} values for the different U-235 depletions shown in Table 9 follow the curves for the majority of the contributors. It should be noted that the results in Figures 8-10 are for standard 23-plate fuel models only. In our analysis, separate models for the 17-plate control fuel assemblies were used. These generate significantly lower k_{∞} values. This approach was not used in the Reference 1 studies.

4.3 DONJON Model Eigenvalues

Table 10 summarizes the k_{eff} values from the core models for the different fuel types at the various stages of core burnup. The BOL and EOL results are presented in both "equal % U-235 depletion" and "equal MWd" exposures, as both were included in the previously published results.

The agreement between the DRAGON/DONJON and ANL-98 (using the WIMS-D4M/DIF3D and MCNP codes) is quite good for the HEU and LEU fresh core cases. These were the only cases reported from the ANL-98 study. The DRAGON/DONJON results are in fair agreement (within 16 mk worst case and typically within 10 mk) with the other groups' results except for the JAERI results. The results from the JAERI analysis did not agree very well with those from the other contributors, as noted in Reference 1.

Tables 12 and 13 show the reactivity loss due to burnup and the reactivity change with enrichment respectively. The DRAGON/DONJON results are in good agreement with the previously published results in both cases.

The discrepancy in the k_{eff} absolute values may be due in part to the use of different cross section libraries as well as modelling approaches. An ENDF/B-V-based library was used in this study whereas the contributors from Reference 1 (ANL-79, INTERATOM, EIR, OSGAE, CEA, CNEA and JAERI) all used older cross section libraries. In addition to this, most other groups modelled the standard fuel and control fuel using a common "half-plate" fuel model whereas multi-plate (half-assembly) fuel models, specific to the standard and control fuel, were used in this analysis. This is discussed in more detail in Section 5.

4.4 Required Flux Plots

The required X & Y midplane flux plots are shown in Figures 11-14 for the HEU core at BOL and EOL exposure for both the DRAGON/DONJON models and the previously published ANL-79 study based on EPRI-CELL/DIF2D. The agreement is very good in all four plots with the ANL-79 results showing a slightly higher epithermal (group 2) flux.

Figures 15-22 show the required flux-ratio plots comparing the MEU:HEU and LEU:HEU flux ratios along the X & Y-axis for equal MWd exposure BOL and EOL cores. Both the

DRAGON/DONJON and the ANL-79 EPRI-CELL/DIF2D plots are shown. As with the flux plots, there is good agreement between the DRAGON/DONJON and ANL-79 results.

5.0 Sensitivity Analysis

There are some differences in the modelling approaches adopted in this study as compared to those used in the previously published work. The impact of these modelling differences on the core eigenvalues and the midplane flux distributions was investigated in an attempt to explain some of the discrepancies between the DRAGON/DONJON results and those published in Reference 1. The changes in core eigenvalue due to the different modelling approaches are summarized in Table 13.

DRAGON half-plate fuel models were created and executed to provide cross section input for the corresponding DONJON core models. DONJON core models were constructed which modelled the control assembly as two separate regions as in the ANL-79 study. The two regions in the ANL-79 models are the "fuel-plate" and the control gap regions. This approach is herein referred to as the "divided" control-assembly approach.

By changing from a divided control-assembly model to a completely homogenized control-assembly model (referred to in Table 13 as the "complete" approach) an increase in the core eigenvalue of ~ 3-4 mk can be expected. The higher enrichment cores show slightly larger changes in k_{eff} than the lower enrichment cores. This modelling change results in changes in the midplane flux distributions of < 2% in the thermal group, with smaller changes in the epithermal and fast group fluxes.

It should be noted that a minor change in the X-direction mesh in the core models was required to accommodate the divided control-assembly modelling approach. The impact of this mesh change on the core eigenvalue and the midplane 3-group flux distributions was found to be minor (< 0.1 mk and < 1% in all groups respectively).

In addition to this, a set of core models using cross section data from specific standard and control fuel half-plate models and complete assembly homogenization was also constructed. The methodology used in these latter cases is identical to that used with the multi-plate models to report the benchmark results in this study.

The change in modelling, from using half-plate to multi-plate cell models (with complete assembly homogenization), can be seen to result in a negative shift in the core eigenvalues. This is on the order of 9-11.5 mk, again with a slightly larger shift in k_{eff} for the higher enrichment cores relative to the lower enrichment cores.

When combined, the two modelling changes result in an overall negative shift in k_{eff} on the order of 7 mk. In addition to this, the multi-plate modelling approach results in slightly higher midplane flux values. The difference is < 2% in the fast and epithermal energy groups and is uniform across the geometry. The thermal flux difference tends to be larger in the fuel regions (5-7% maximum) with slightly larger discrepancies in the lower enrichment cores relative to the higher enrichment cores. The differences are weakly burnup dependent.

It should be noted that the relative changes in the core multiplication factors due to burnup and with enrichment are only slightly effected by the differences in the previously mentioned

modelling approaches (< 1 mk). This is consistent with the comparison of results with the previously published data.

The differences between the DRAGON/DONJON results and those found in the MNR-98 study using the WIMS-AECL/3DDT code package can in part be attributed to the fact that the MNR-98 WIMS-AECL calculations used a 34-group structure for the fuel calculations. Previous work has shown the use of 34-groups rather than the maximum 89-groups in WIMS-AECL 1-D infinite slab fuel models gives a positive bias to the diffusion theory results on the order of 2 mk for an HEU core and 6 mk for an LEU core[9].

6.0 Conclusions

The results of this analysis show that the DRAGON/DONJON code package and the methodology used herein are suitable for static modelling of plate-fueled research reactors and for reduced-enrichment-related analysis for these types of systems.

The agreement between DRAGON/DONJON generated eigenvalue and flux-distribution results and those from previously published work (Reference 1) is good with any discrepancies likely attributable to differences in microscopic cross section libraries or modelling details. Despite some differences in the absolute core eigenvalues generated by DRAGON/DONJON when compared to those reported in previously published studies, the respective relative changes with burnup and enrichment change are in good agreement.

This benchmark problem is simply the first step in the development of models and methodology suitable for MNR, using the DRAGON/DONJON code package. The modelling approach validated in this study is based on 1-D infinite-slab multi-plate fuel models. The development and exploration of explicit 2-D fuel and irradiation-site transport theory models are left as a future exercise.

7.0 Acknowledgments

The author would like to thank Bill Garland of McMaster University for authorizing and funding this work as well as Guy Marleau and Elisabeth Varin of École Polytechnique de Montréal for their patience and help in learning the DRAGON and DONJON codes.

8.0 References

1. IAEA-TECDOC-233, “Research Reactor Core Conversion From the Use of Highly Enriched Uranium to the Use of Low Enriched Uranium Fuels Guidebook”, IAEA, 1980.
2. H. S. Al-Basha, “Validation of WIMS-AECL/3DDT Code Package for MNR Fuel Conversion Analysis Using the IAEA 10 MW Benchmark Problem”, MNR-TR-1998-02, May 1998.
3. G. Marleau, A. Hébert, R. Roy, “A User’s Guide for DRAGON Version DRAGON_980911 Release 3.03”, Technical Report IGE-174 Rev. 4, Institut de génie nucléaire, Départment de génie mécanique, École Polytechnique de Montréal, September 1998.
4. A. Hébert, G. Marleau, R. Roy, “A Description of the DRAGON Data Structures”, Technical Report IGE-232 Rev. 1, Institut de génie nucléaire, Départment de génie mécanique, École Polytechnique de Montréal, September 1998.

5. E. Varin, A. Hébert, R. Roy, J. Koclas, “A User’s Guide for DONJON Version DONJON_980202 Release 2.00”, Technical Report IGE-208 Rev. 2, École Polytechnique de Montréal, Institut de génie nucléaire, February 1999.
6. E. Varin, A. Hébert, “Linked List Specifications for DONJON”, Technical Report IGE-226 Rev. 2, École Polytechnique de Montréal, Institut de génie nucléaire, February 1999.
7. J. Griffiths, “WIMS-AECL User’s Manual”, AECL RC-1176, COG-94-52, March 1994.
8. M. T. Sissaoui, J. Koclas, A. Hébert, “Solution of the Improved and Generalized Quasistatic Methods by Kaps and Rentrop Integration Scheme with Stepsize Control”, Ann. Nucl. Energy, Vol. 22, No. 12, pp. 763-774, 1995.
9. S. E. Day, “Review of the Reactor Physics NDEC Dataset and Modelling”, MNR Technical Report 1999-04, April 16, 1999.

9.0 Tables

Table 1: IAEA 10 MW Benchmark Specifications (from Appendix F-0 of Reference 1)

Specifications

Aims: Comparison of the different calculation methods and cross-section data sets used in different laboratories, limited conclusions for real conversion problems.

Table 1 Specifications for the Methodical Benchmark-Problem

Data and Specifications Agreed Upon:

Active Core Height 600 mm
Extrapolation Length 80 mm (in 80 mm distance from the core, the cosine-shaped flux goes to zero)
X-Y Calculations only

Space at the grid plate per fuel element 77 mm x 81 mm

Fuel element cross-section
76 mm x 80.5 mm including support plate
76 mm x 80.0 m without support plate

Meat dimensions
63 mm x 0.51 mm x 600 mm

Aluminum-canning with $\rho_{Al} = 2.7\ g \cdot cm^{-3}$

Thickness of support plate 4.75 mm; $\rho_{Al} = 2.7\ g \cdot cm^{-3}$

Number of fuel plates per fuel element:
23 identical plates, each 1.27 mm thick

Number of fuel plates per control element:
17 identical plates, each 1.27 mm thick

Identification of the remaining plate positions of the control element:
4 plates of pure aluminum $\rho_{Al} = 1.7\ g \cdot cm^{-3}$, each 1.27 mm thick in the position of the first, the third, the twenty-first, and the twenty-third standard plate position; water gaps between the two sets of aluminum plates.

Specifications of the different fuels (UAl_x-Al Fuel) for HEU, MEU, LEU corresponding to the previous definitions:

HEU:
- Enrichment 93 w/o (weight %) U-235
- 280 g U-235 per fuel element, which corresponds to 12.174 g U-235 per each fuel plate
- 21 w/o of uranium in the UAl_x-Al
- only U-235 and U-238 in the fresh fuel

MEU:
- Enrichment 45 w/o U-235
- 320 g U-235 per fuel element (23 plates)
- 40 w/o of uranium in the UAl_x-Al
- only U-235 and U-238 in the fresh fuel

LEU:
- Enrichment 20 w/o U-235
- 390 g U-235 per fuel element (23 plates)
- 72 w/o of uranium in the UAl_x-Al
- only U-235 and U-238 in the fresh fuel

Total power: 10 MW_{th} (power buildup by 3.1×10^{10} fission/Joule)

Thermal hydraulic data:
Water temperature 20°C
Fuel temperature 20°C
Pressure at core height 1.7 bar

Xenon-State:
Homogeneous Xenon content corresponding to average-power-density

Results

k_{eff}; fluxes and flux ratios along the two symmetry-axes of the core in three groups and for begin of cycle (BOL) and end of cycle (EOL), respectively.

$\phi_{thermal}$ with $0\ eV < E_n < 0.625\ eV$

$\phi_{epithermal}$ with $0.625\ eV < E_n < 5.531\ keV$

ϕ_{fast} with $E_n > 5.531\ keV$

Table 2: Energy Group Structures for the IAEA 10 MW Benchmark Problem

5-group Structure			3-group Structure		
Energy Group	Energy Bounds (eV)		Energy Group	Energy Bounds (eV)	
	Lower	Upper		Lower	Upper
1	8.21×10^5	10×10^6	1	5.53×10^3	10×10^6
2	5.53×10^3	8.21×10^5			
3	1.855	5.53×10^3	2	0.625	5.53×10^3
4	0.625	1.855			
5	0.0	0.625	3	0.0	0.625

Table 3: Average Isotope Atom Densities in the Fuel Meat for HEU Standard Fuel Model

% Burn-Up	Average Isotope Atom Density in Fuel (/bcm)								
	U-235	U-236	U-238	Pu-239	Pu-240	Pu-241	Pu-242	Xe-135	Sm-149
0	1.6180E-03	0.0000E+00	1.2030E-04	0.0000E+00	0.0000E+00	0.0000E+00	0.0000E+00	0.0000E+00	0.0000E+00
5	1.5370E-03	1.3570E-05	1.1990E-04	3.2050E-07	8.9001E-09	3.8334E-10	3.2628E-12	1.6504E-08	1.2822E-07
10	1.4561E-03	2.7050E-05	1.1949E-04	6.4646E-07	3.3287E-08	2.9200E-09	5.3026E-11	1.5747E-08	1.2668E-07
15	1.3752E-03	4.0455E-05	1.1907E-04	9.3162E-07	6.9380E-08	9.1582E-09	2.6426E-10	1.4978E-08	1.2461E-07
20	1.2943E-03	5.3773E-05	1.1865E-04	1.1785E-06	1.1451E-07	2.0092E-08	8.1774E-10	1.4198E-08	1.2240E-07
25	1.2134E-03	6.7010E-05	1.1822E-04	1.3893E-06	1.6652E-07	3.6285E-08	1.9554E-09	1.3407E-08	1.1976E-07
30	1.1325E-03	8.0160E-05	1.1778E-04	1.5661E-06	2.2357E-07	5.7911E-08	3.9768E-09	1.2604E-08	1.1665E-07
35	1.0516E-03	9.3215E-05	1.1733E-04	1.7098E-06	2.8400E-07	8.4805E-08	7.2377E-09	1.1790E-08	1.1307E-07
40	9.7074E-04	1.0618E-04	1.1688E-04	1.8226E-06	3.4637E-07	1.1649E-07	1.2154E-08	1.0962E-08	1.0902E-07
45	8.8985E-04	1.1903E-04	1.1641E-04	1.9049E-06	4.0940E-07	1.5218E-07	1.9202E-08	1.0125E-08	1.0452E-07
50	8.0895E-04	1.3179E-04	1.1592E-04	1.9590E-06	4.7192E-07	1.9092E-07	2.8934E-08	9.2753E-09	9.9588E-08

Table 4: Average Isotope Atom Densities in the Fuel Meat for HEU Control Fuel Model

% Burn-Up	Average Isotope Atom Density in Fuel (/bcm)								
	U-235	U-236	U-238	Pu-239	Pu-240	Pu-241	Pu-242	Xe-135	Sm-149
0	1.6180E-03	0.0000E+00	1.2030E-04	0.0000E+00	0.0000E+00	0.0000E+00	0.0000E+00	0.0000E+00	0.0000E+00
5	1.5370E-03	1.3167E-05	1.1999E-04	2.4799E-07	6.3713E-09	2.2499E-10	1.8918E-12	1.5953E-08	1.2442E-07
10	1.4561E-03	2.6257E-05	1.1967E-04	5.0206E-07	2.4166E-08	1.7375E-09	3.1218E-11	1.5236E-08	1.2234E-07
15	1.3752E-03	3.9289E-05	1.1935E-04	7.2674E-07	5.1034E-08	5.5170E-09	1.5749E-10	1.4506E-08	1.1960E-07
20	1.2943E-03	5.2257E-05	1.1903E-04	9.2353E-07	8.5328E-08	1.2254E-08	4.9316E-10	1.3764E-08	1.1679E-07
25	1.2134E-03	6.5160E-05	1.1869E-04	1.0937E-06	1.2567E-07	2.2403E-08	1.1929E-09	1.3010E-08	1.1369E-07
30	1.1325E-03	7.7988E-05	1.1835E-04	1.2382E-06	1.7081E-07	3.6199E-08	2.4533E-09	1.2244E-08	1.1026E-07
35	1.0516E-03	9.0750E-05	1.1800E-04	1.3583E-06	2.1969E-07	5.3697E-08	4.5179E-09	1.1465E-08	1.0648E-07
40	9.7074E-04	1.0344E-04	1.1763E-04	1.4550E-06	2.7130E-07	7.4744E-08	7.6782E-09	1.0672E-08	1.0236E-07
45	8.8984E-04	1.1604E-04	1.1726E-04	1.5287E-06	3.2469E-07	9.9001E-08	1.2279E-08	9.8673E-09	9.7905E-08
50	8.0895E-04	1.2856E-04	1.1687E-04	1.5802E-06	3.7901E-07	1.2601E-07	1.8738E-08	9.0489E-09	9.3126E-08

Table 5: Average Isotope Atom Densities in the Fuel Meat for MEU Standard Fuel Model

% Burn-Up	Average Isotope Atom Density in Fuel (/bcm)								
	U-235	U-236	U-238	Pu-239	Pu-240	Pu-241	Pu-242	Xe-135	Sm-149
0	1.8500E-03	0.0000E+00	2.2320E-03	0.0000E+00	0.0000E+00	0.0000E+00	0.0000E+00	0.0000E+00	0.0000E+00
5	1.7574E-03	1.5751E-05	2.2272E-03	3.9063E-06	8.3832E-08	3.7799E-09	3.1549E-11	1.8694E-08	1.4854E-07
10	1.6649E-03	3.1402E-05	2.2222E-03	7.8748E-06	3.3519E-07	3.1046E-08	5.5582E-10	1.7933E-08	1.4771E-07
15	1.5724E-03	4.6964E-05	2.2171E-03	1.1406E-05	7.2262E-07	1.0105E-07	2.8807E-09	1.7151E-08	1.4629E-07
20	1.4799E-03	6.2428E-05	2.2119E-03	1.4519E-05	1.2194E-06	2.2699E-07	9.1394E-09	1.6347E-08	1.4453E-07
25	1.3874E-03	7.7800E-05	2.2066E-03	1.7229E-05	1.8030E-06	4.1687E-07	2.2246E-08	1.5524E-08	1.4215E-07
30	1.2949E-03	9.3063E-05	2.2011E-03	1.9551E-05	2.4531E-06	6.7371E-07	4.5832E-08	1.4680E-08	1.3915E-07
35	1.2024E-03	1.0822E-04	2.1954E-03	2.1497E-05	3.1523E-06	9.9636E-07	8.4275E-08	1.3814E-08	1.3552E-07
40	1.1099E-03	1.2326E-04	2.1895E-03	2.3077E-05	3.8853E-06	1.3798E-06	1.4268E-07	1.2930E-08	1.3129E-07
45	1.0174E-03	1.3817E-04	2.1834E-03	2.4303E-05	4.6379E-06	1.8158E-06	2.2695E-07	1.2025E-08	1.2647E-07
50	9.2495E-04	1.5296E-04	2.1771E-03	2.5184E-05	5.3978E-06	2.2932E-06	3.4397E-07	1.1100E-08	1.2109E-07

Table 6: Average Isotope Atom Densities in the Fuel Meat for MEU Control Fuel Model

% Burn -Up	Average Isotope Atom Density in Fuel (/bcm)								
	U-235	U-236	U-238	Pu-239	Pu-240	Pu-241	Pu-242	Xe-135	Sm-149
0	1.8500E-03	0.0000E+00	2.2320E-03	0.0000E+00	0.0000E+00	0.0000E+00	0.0000E+00	0.0000E+00	0.0000E+00
5	1.7574E-03	1.5220E-05	2.2281E-03	3.1793E-06	6.3233E-08	2.3273E-09	1.9351E-11	1.7971E-08	1.4346E-07
10	1.6649E-03	3.0363E-05	2.2241E-03	6.4275E-06	2.5640E-07	1.9360E-08	3.4565E-10	1.7238E-08	1.4175E-07
15	1.5724E-03	4.5429E-05	2.2199E-03	9.3401E-06	5.5984E-07	6.3723E-08	1.8108E-09	1.6486E-08	1.3929E-07
20	1.4799E-03	6.0418E-05	2.2157E-03	1.1929E-05	9.5656E-07	1.4479E-07	5.8072E-09	1.5716E-08	1.3661E-07
25	1.3874E-03	7.5330E-05	2.2114E-03	1.4204E-05	1.4316E-06	2.6897E-07	1.4284E-08	1.4926E-08	1.3351E-07
30	1.2949E-03	9.0160E-05	2.2069E-03	1.6173E-05	1.9714E-06	4.3992E-07	2.9758E-08	1.4117E-08	1.2997E-07
35	1.2024E-03	1.0491E-04	2.2022E-03	1.7844E-05	2.5636E-06	6.5862E-07	5.5338E-08	1.3286E-08	1.2597E-07
40	1.1099E-03	1.1956E-04	2.1974E-03	1.9221E-05	3.1968E-06	9.2359E-07	9.4767E-08	1.2438E-08	1.2154E-07
45	1.0174E-03	1.3411E-04	2.1924E-03	2.0312E-05	3.8605E-06	1.2313E-06	1.5252E-07	1.1569E-08	1.1669E-07
50	9.2495E-04	1.4857E-04	2.1872E-03	2.1121E-05	4.5450E-06	1.5761E-06	2.3399E-07	1.0679E-08	1.1141E-07

Table 7: Average Isotope Atom Densities in the Fuel Meat for LEU Standard Fuel Model

% Burn -Up	Average Isotope Atom Density in Fuel (/bcm)								
	U-235	U-236	U-238	Pu-239	Pu-240	Pu-241	Pu-242	Xe-135	Sm-149
0	2.2540E-03	0.0000E+00	8.9020E-03	0.0000E+00	0.0000E+00	0.0000E+00	0.0000E+00	0.0000E+00	0.0000E+00
5	2.1412E-03	1.9668E-05	8.8885E-03	1.0839E-05	2.3502E-07	1.2081E-08	1.0285E-10	2.2433E-08	1.8577E-07
10	2.0285E-03	3.9225E-05	8.8746E-03	2.1650E-05	9.3241E-07	9.8516E-08	1.7993E-09	2.1688E-08	1.8669E-07
15	1.9158E-03	5.8676E-05	8.8603E-03	3.1332E-05	2.0018E-06	3.1906E-07	9.2743E-09	2.0905E-08	1.8665E-07
20	1.8031E-03	7.8011E-05	8.8454E-03	3.9932E-05	3.3675E-06	7.1318E-07	2.9275E-08	2.0086E-08	1.8589E-07
25	1.6904E-03	9.7225E-05	8.8300E-03	4.7492E-05	4.9662E-06	1.3027E-06	7.0856E-08	1.9233E-08	1.8420E-07
30	1.5777E-03	1.1631E-04	8.8140E-03	5.4047E-05	6.7448E-06	2.0935E-06	1.4518E-07	1.8342E-08	1.8156E-07
35	1.4650E-03	1.3525E-04	8.7974E-03	5.9630E-05	8.6578E-06	3.0790E-06	2.6537E-07	1.7419E-08	1.7805E-07
40	1.3523E-03	1.5405E-04	8.7800E-03	6.4276E-05	1.0668E-05	4.2427E-06	4.4671E-07	1.6461E-08	1.7367E-07
45	1.2396E-03	1.7269E-04	8.7619E-03	6.8008E-05	1.2740E-05	5.5568E-06	7.0639E-07	1.5468E-08	1.6844E-07
50	1.1269E-03	1.9115E-04	8.7428E-03	7.0848E-05	1.4846E-05	6.9872E-06	1.0644E-06	1.4437E-08	1.6235E-07

Table 8: Average Isotope Atom Densities in the Fuel Meat for LEU Control Fuel Model

% Burn -Up	Average Isotope Atom Density in Fuel (/bcm)								
	U-235	U-236	U-238	Pu-239	Pu-240	Pu-241	Pu-242	Xe-135	Sm-149
0	2.2540E-03	0.0000E+00	8.9020E-03	0.0000E+00	0.0000E+00	0.0000E+00	0.0000E+00	0.0000E+00	0.0000E+00
5	2.1412E-03	1.8889E-05	8.8910E-03	8.8677E-06	1.7812E-07	7.4283E-09	6.3536E-11	2.1362E-08	1.7783E-07
10	2.0285E-03	3.7684E-05	8.8797E-03	1.7752E-05	7.1672E-07	6.1262E-08	1.1251E-09	2.0621E-08	1.7713E-07
15	1.9158E-03	5.6389E-05	8.8680E-03	2.5760E-05	1.5593E-06	2.0060E-07	5.8619E-09	1.9850E-08	1.7529E-07
20	1.8031E-03	7.4999E-05	8.8559E-03	3.2920E-05	2.6571E-06	4.5356E-07	1.8708E-08	1.9048E-08	1.7294E-07
25	1.6904E-03	9.3509E-05	8.8434E-03	3.9260E-05	3.9676E-06	8.3812E-07	4.5786E-08	1.8216E-08	1.6995E-07
30	1.5777E-03	1.1191E-04	8.8304E-03	4.4799E-05	5.4537E-06	1.3628E-06	9.4873E-08	1.7352E-08	1.6629E-07
35	1.4650E-03	1.3020E-04	8.8169E-03	4.9560E-05	7.0832E-06	2.0286E-06	1.7544E-07	1.6458E-08	1.6201E-07
40	1.3523E-03	1.4837E-04	8.8028E-03	5.3563E-05	8.8268E-06	2.8289E-06	2.9874E-07	1.5534E-08	1.5711E-07
45	1.2396E-03	1.6642E-04	8.7879E-03	5.6823E-05	1.0660E-05	3.7509E-06	4.7810E-07	1.4576E-08	1.5161E-07
50	1.1270E-03	1.8433E-04	8.7723E-03	5.9353E-05	1.2558E-05	4.7760E-06	7.2929E-07	1.3585E-08	1.4550E-07

Table 9: DRAGON Fuel Model Eigenvalues for Equal Percent U-235 Burnup.

% Burn-Up	k_∞					
	Standard Fuel			Control Fuel		
	HEU	MEU	LEU	HEU	MEU	LEU
5	1.64282	1.6082	1.56441	1.49383	1.48407	1.47109
10	1.6222	1.58845	1.54492	1.47218	1.46353	1.45138
15	1.60072	1.56781	1.5244	1.44958	1.4421	1.43066
20	1.57795	1.54595	1.50272	1.4256	1.41932	1.40876
25	1.55354	1.5226	1.47977	1.39986	1.39495	1.38533
30	1.52715	1.49753	1.45542	1.37209	1.36868	1.3603
35	1.49837	1.47046	1.42946	1.3418	1.34017	1.33337
40	1.46679	1.44097	1.4017	1.30875	1.30922	1.30426
45	1.43179	1.40864	1.37179	1.27226	1.2752	1.27277
50	1.39263	1.37287	1.33933	1.23163	1.23766	1.23824

Table 10: Core Model Eigenvalues

Enrichment (%)	Core	MNR[(1)] DONJON	MNR-98[(1)] 3DDT	ANL-98[(1)] DIF3D	ANL-98[(1)] MCNP	ANL-79[(2)] DIF2D	ANL-79[(1)] MCNP
93	BOL	1.0307	1.0274			1.0233	
93	EOL	1.0075	1.0037			1.0004	
93	Fresh	1.1919	1.1899	1.1940	1.1924	1.1834	1.1890
45	BOL (MWD)	1.0472				1.0410	
45	EOL (MWD)	1.0302				1.0238	
45	BOL (%)	1.0302				1.0247	
45	EOL (%)	1.0087				1.0033	
45	Fresh	1.1843				1.1782	
20	BOL (MWD)	1.0613	1.0658			1.0540	
20	EOL (MWD)	1.0493	1.0531			1.0419	
20	BOL (%)	1.0275	1.0323			1.0213	
20	EOL (%)	1.0075	1.0115			1.0014	
20	Fresh	1.1752	1.1813	1.1774	1.1737	1.1683	1.1680
Enrichment (%)	**Core**	**Germany[(2)] INTERATOM**	**Switz[(2)] EIR**	**Austria[(2)] OSGAE**	**France[(2)] CEA**	**Argentina[(2)] CNEA**	**Japan[(2)] JAERI**
93	BOL	1.0328	1.0368	1.0320	1.0404	1.0377	1.0420
93	EOL	1.0101	1.0138	1.0090	1.0170	1.0143	1.0220
93	Fresh	1.1888	1.1939	1.1966	1.2020	1.2002	1.1810
45	BOL (MWD)	1.0474					
45	EOL (MWD)	1.0309					
45	BOL (%)	1.0311	1.0306	1.0334	1.0408		1.0489
45	EOL (%)	1.0108	1.0099	1.0116	1.0190		1.0306
45	Fresh	1.1790	1.1791	1.1896	1.1950		1.1811
20	BOL (MWD)	1.0599					
20	EOL (MWD)	1.0485					
20	BOL (%)	1.0278	1.0178	1.0320	1.0394	1.0332	1.0578
20	EOL (%)	1.0091	1.0000	1.0120	1.0191	1.0130	1.0412
20	Fresh	1.1683	1.1594	1.1813	1.1870	1.1815	1.1834

Note: calculations are based on either (1) 3-D or (2) 2-D core models

Table 11: Reactivity Loss due to Burnup

Enrichment (%)	Equal burnup in	Reactivity, ρ (mk) ≡ $(1/k_{BOL} - 1/k_{EOL}) * 1000$				
		MNR[(1)] DONJON	**MNR-98[(1)] 3DDT**	**ANL-79[(2)] DIF2D**	**Germany[(2)] INTERATOM**	**Switz[(2)] EIR**
93 w/o	MWd = %	-22.3	-23.0	-22.4	-21.8	-21.9
45 w/o	MWd	-15.8		-16.1	-15.3	
	%	-20.7		-20.8	-19.5	-19.9
20 w/o	MWd	-10.8	-11.3	-11.0	-10.3	
	%	-19.3	-19.9	-19.5	-18.0	-17.5
Enrichment (%)	**Equal burnup in**	**Austria[(2)] OSGAE**	**France[(2)] CEA**	**Argentina[(2)] CNEA**	**Japan[(2)] JAERI**	
93 w/o	MWd = %	-22.1	-22.1	-22.2	-18.8	
45 w/o	MWd					
	%	-20.9	-20.6		-16.9	
20 w/o	MWd					
	%	-19.2	-19.2	-19.3	-15.1	

Note: calculations are based on either (1) 3-D or (2) 2-D core models

Table 12: Reactivity Change with Enrichment

Enrichment Change	Core	Reactivity, ρ (mk) ≡ $(1/k_1 - 1/k_2) * 1000$					
		MNR[(1)] DONJON	**MNR-98[(1)] 3DDT**	**ANL-98[(1)] DIF3D**	**ANL-98[(1)] MCNP**	**ANL-79[(2)] DIF2D**	**ANL-79[(2)] MCNP**
93 -> 45	Fresh	-5.4				-3.7	
	BOL (%)	-0.5				1.3	
	BOL (MWD)	15.3				16.6	
	EOL (%)	1.1				2.9	
	EOL (MWD)	21.8				22.8	
93 -> 20	Fresh	-11.9	-6.1	-11.8	-13.4	-10.9	-15.1
	BOL (%)	-3.0	4.6			-1.9	
	BOL (MWD)	28.0	35.1			28.5	
	EOL (%)	0.0	7.7			1.0	
	EOL (MWD)	39.5	46.7			39.8	
Enrichment Change	**Core**	**Germany[(2)] INTERATOM**	**Switz[(2)] EIR**	**Austria[(2)] OSGAE**	**France[(2)] CEA**	**Argentina[(2)] CNEA**	**Japan[(2)] JAERI**
93 -> 45	Fresh	-7.0	-10.5	-4.9	-4.9		0.1
	BOL (%)	-1.6	-5.8	1.3	0.4		6.3
	BOL (MWD)	13.5					
	EOL (%)	0.7	-3.8	2.5	1.9		8.2
	EOL (MWD)	20.0					
93 -> 20	Fresh	-14.8	-24.9	-10.8	-10.5	-13.2	1.7
	BOL (%)	-4.7	-18.0	0.0	-0.9	-4.2	14.3
	BOL (MWD)	24.8					
	EOL (%)	-1.0	-13.6	2.9	2.0	-1.3	18.0
	EOL (MWD)	36.3					

Note: calculations are based on either (1) 3-D or (2) 2-D core models

Table 13: Changes in Core Eigenvalue due to Changes in Modelling

Enrichment	Core	k_{eff}	Δk_{eff}		
		DONJON (multi-plate)	**Divided Half-Plate → Complete Half-Plate**	**Complete Half-Plate → Complete Multi-Plate**	**Divided Half-Plate → Complete Multi-Plate**
93	BOL	1.0307	4.3	-11.3	-7.0
93	EOL	1.0075	4.2	-11.2	-7.0
93	Fresh	1.1919	4.1	-11.4	-7.3
45	BOL (%)	1.0302	3.7	-10.7	-7.0
45	EOL (%)	1.0087	3.7	-10.8	-7.1
45	Fresh	1.1843	3.5	-10.5	-7.0
20	BOL (%)	1.0275	3.1	-9.8	-6.8
20	EOL (%)	1.0075	3.0	-10.0	-7.0
20	Fresh	1.1752	2.8	-9.2	-6.5

10.0 Figures

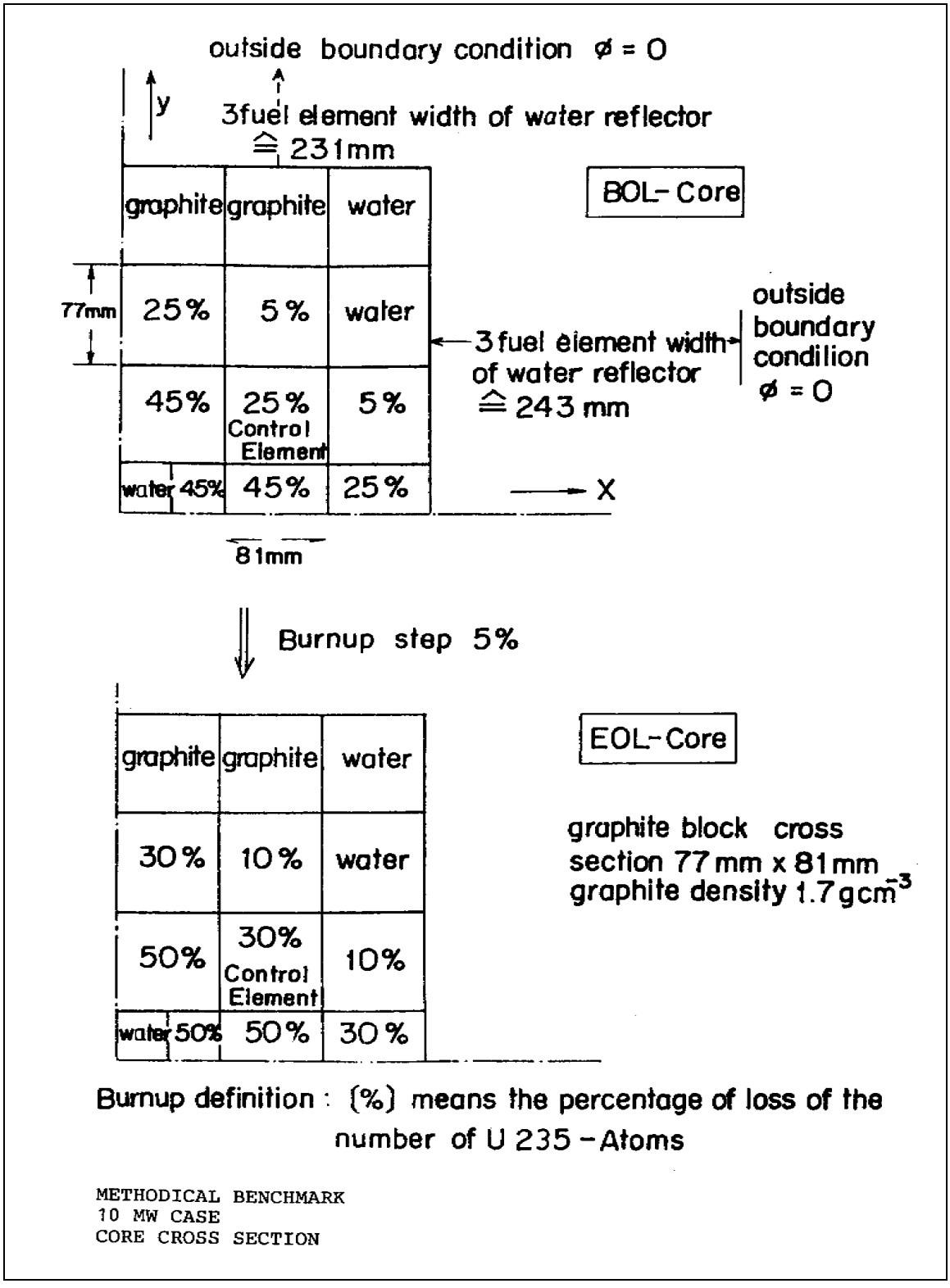

Figure 1: IAEA 10 MW Benchmark Core Description (from Appendix F-0 of Reference 1)

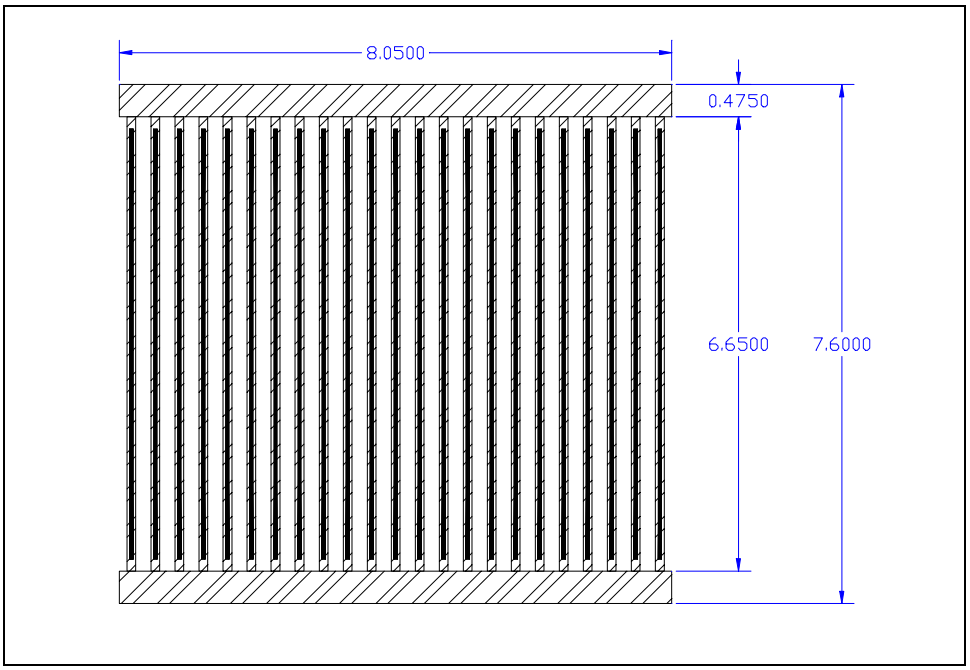

Figure 2: Cross Sectional View of IAEA 23-Plate Standard Fuel Assembly. Filled regions represent fuel and hatched regions represent aluminum.

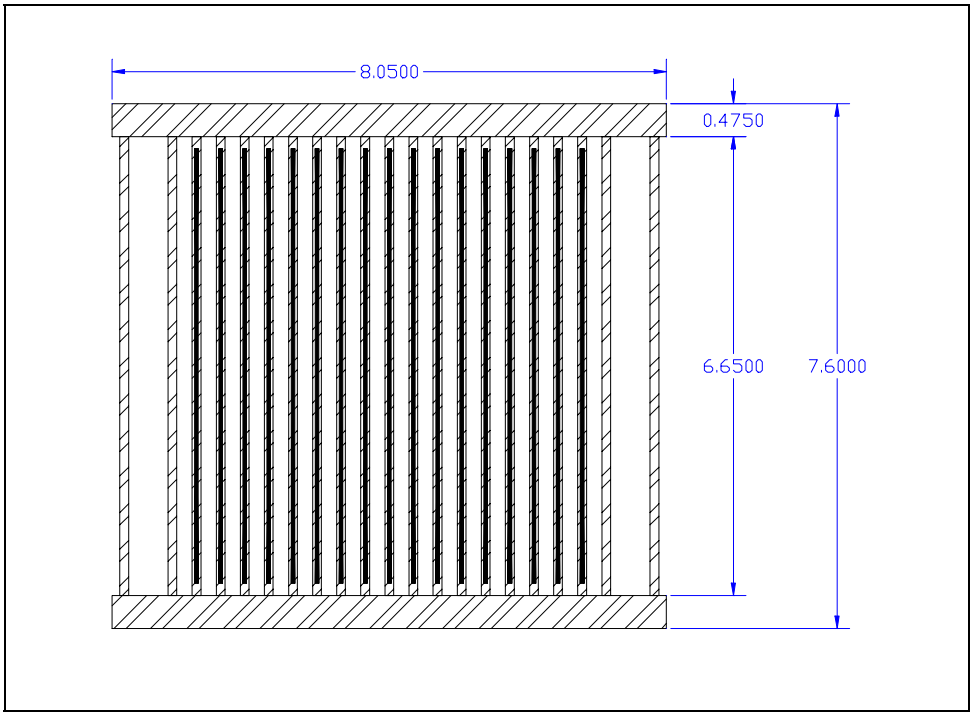

Figure 3: Cross Sectional View of IAEA 17-Plate Control Fuel Assembly. Filled regions represent fuel and hatched regions represent aluminum. Note: The control fuel assembly is similar to the standard fuel assembly with plate numbers 1,3,21, and 23 replaced by aluminum plates and plate numbers 2 and 22 removed.

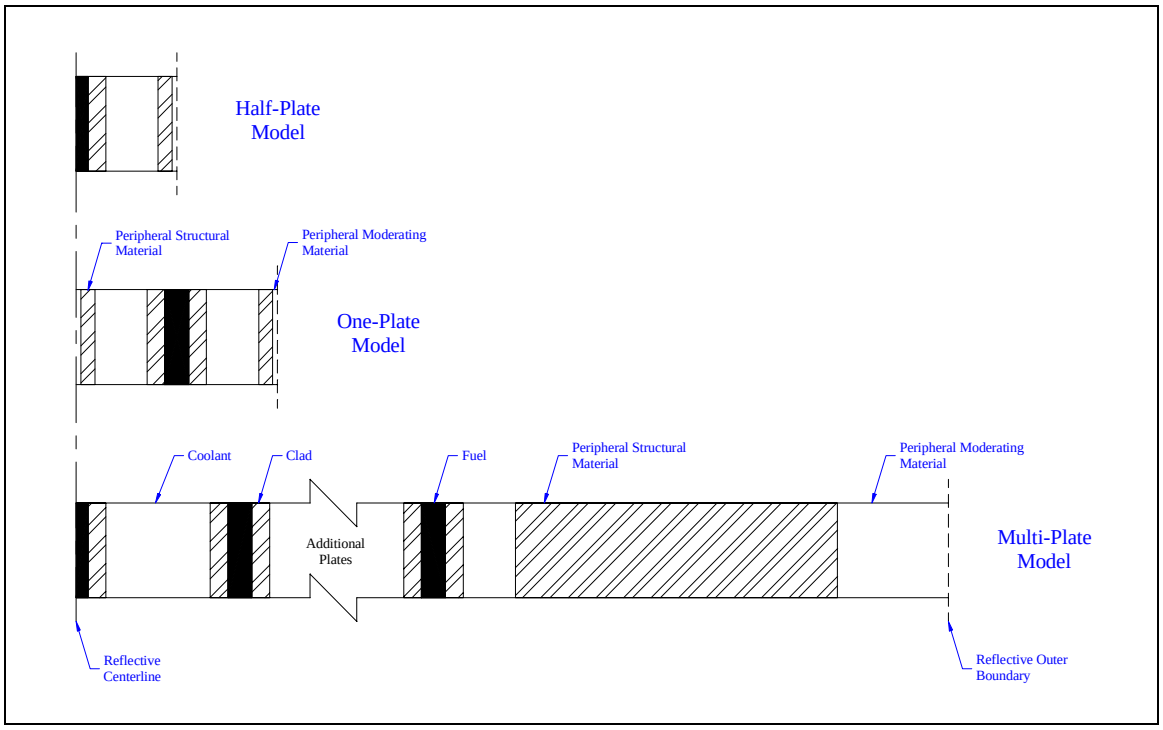

Figure 4: One-Dimensional Infinite Slab Models for IAEA 23-Plate Standard Fuel

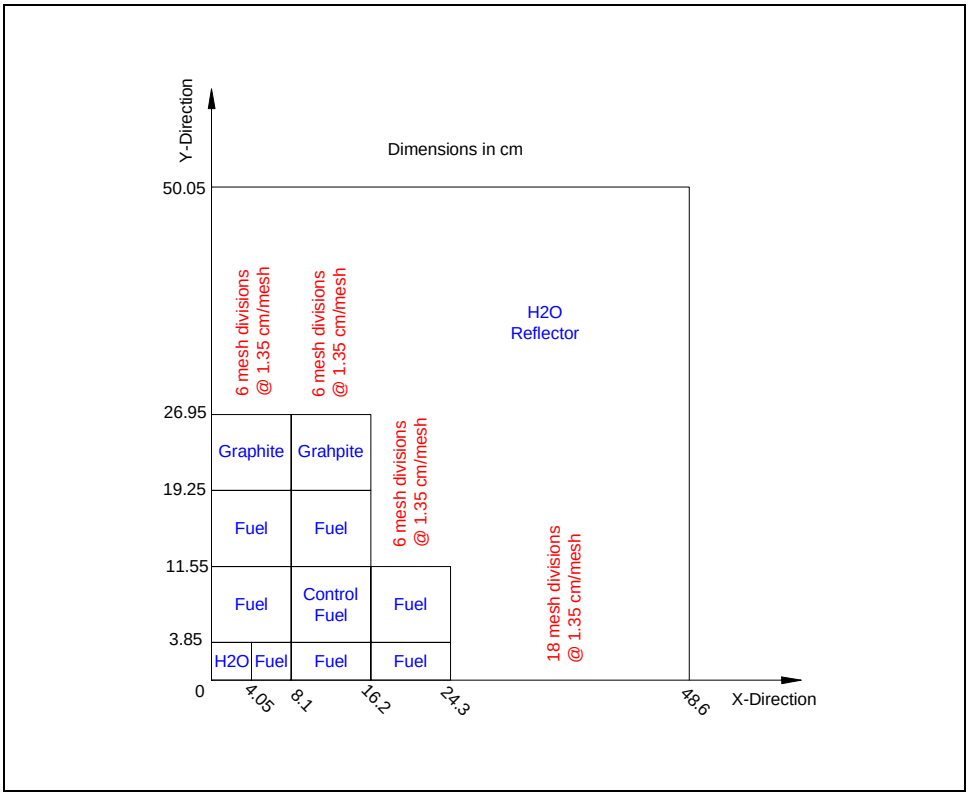

Figure 5: Spatial Mesh in the X-Direction for the IAEA 10 MW Benchmark Problem

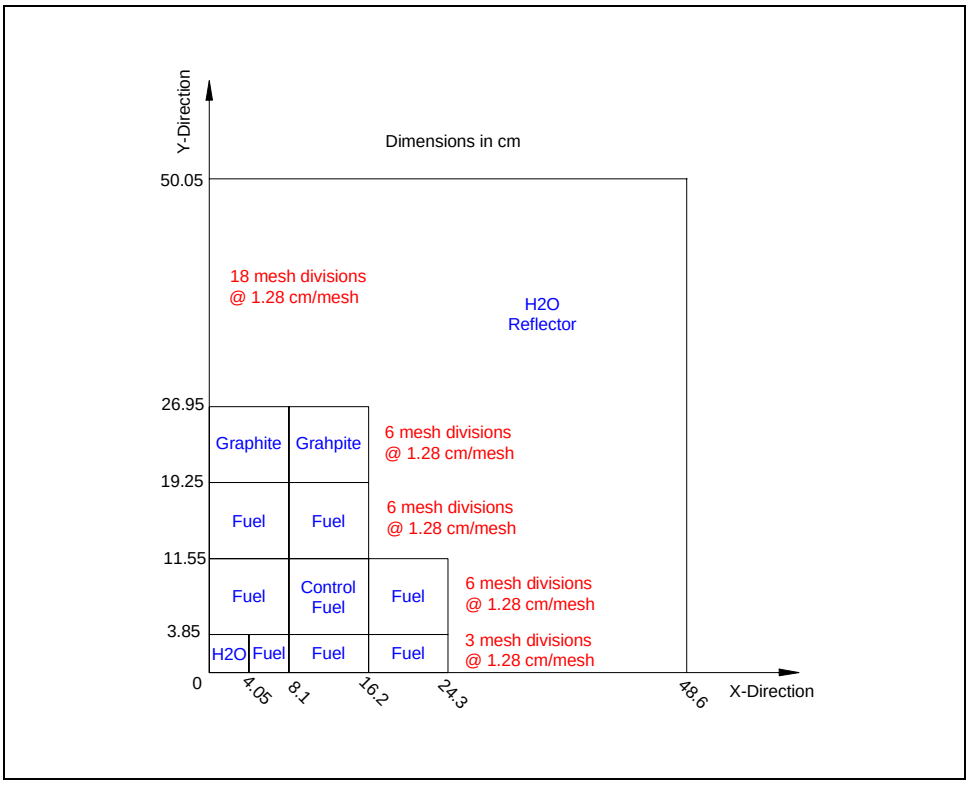

Figure 6: Spatial Mesh in the Y-Direction for the IAEA 10 MW Benchmark Problem

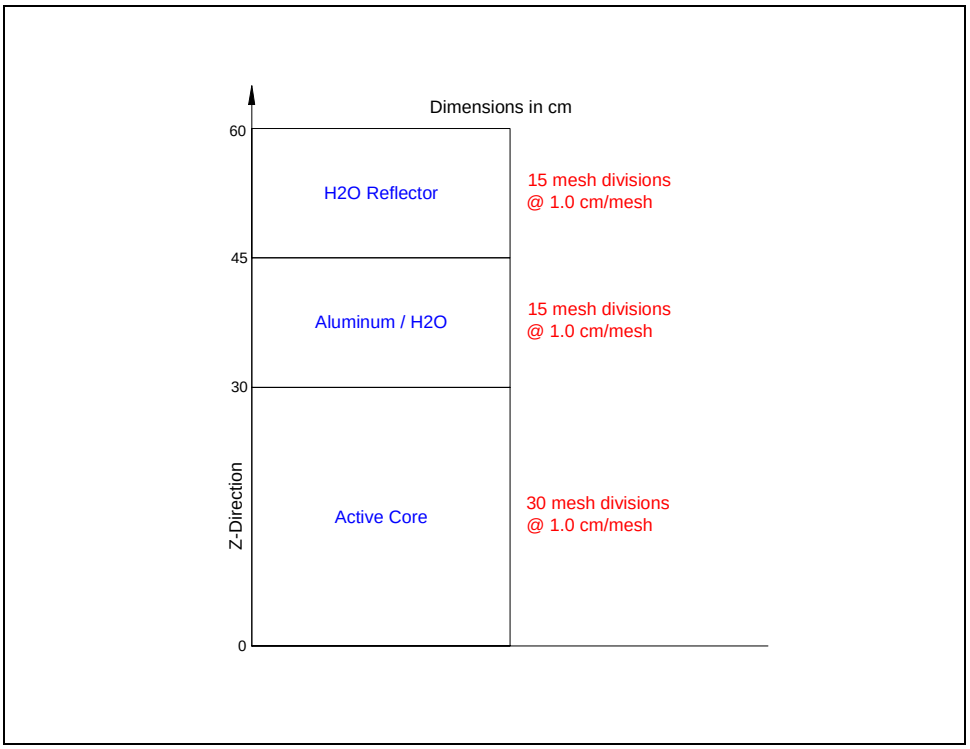

Figure 7: Spatial Mesh in the Z-Direction for the IAEA 10 MW Benchmark Problem

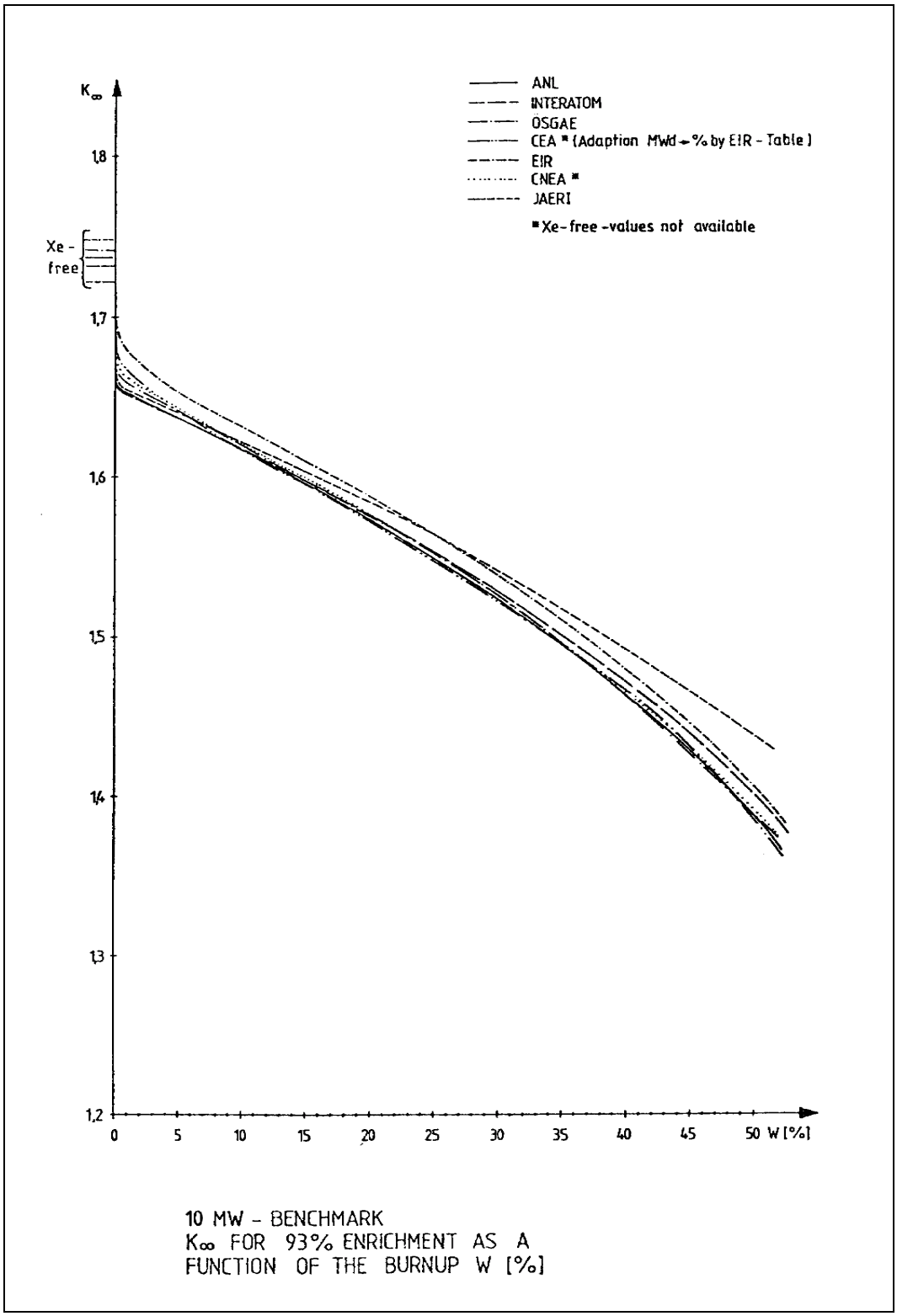

Figure 8: k_∞ for HEU Enrichment as a Function of U-235 Burnup (Reproduced from Reference 1)

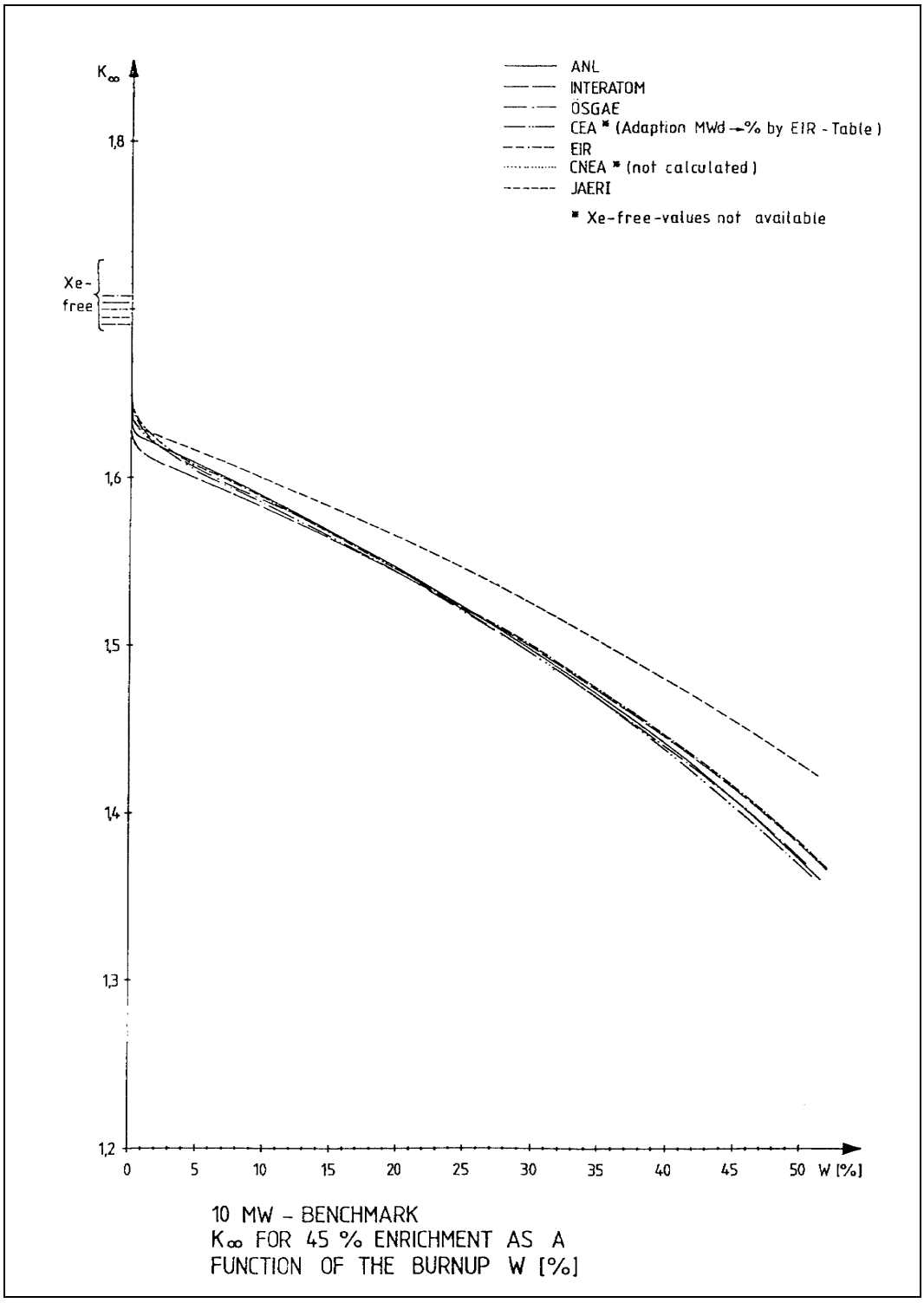

Figure 9: k_∞ for MEU Enrichment as a Function of U-235 Burnup (Reproduced from Reference 1)

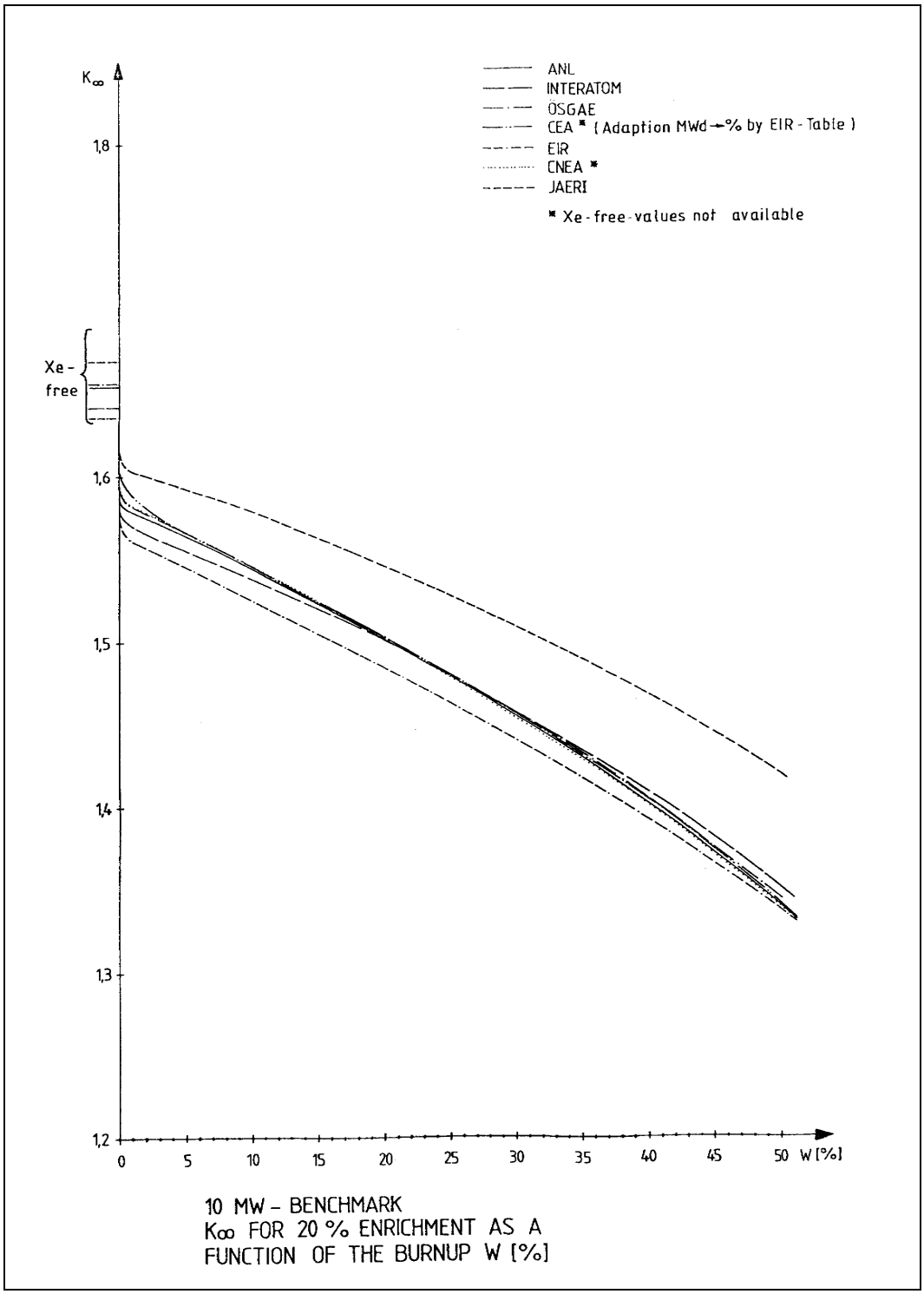

Figure 10: k_∞ for LEU Enrichment as a Function of U-235 Burnup (Reproduced from Reference 1)

(a)

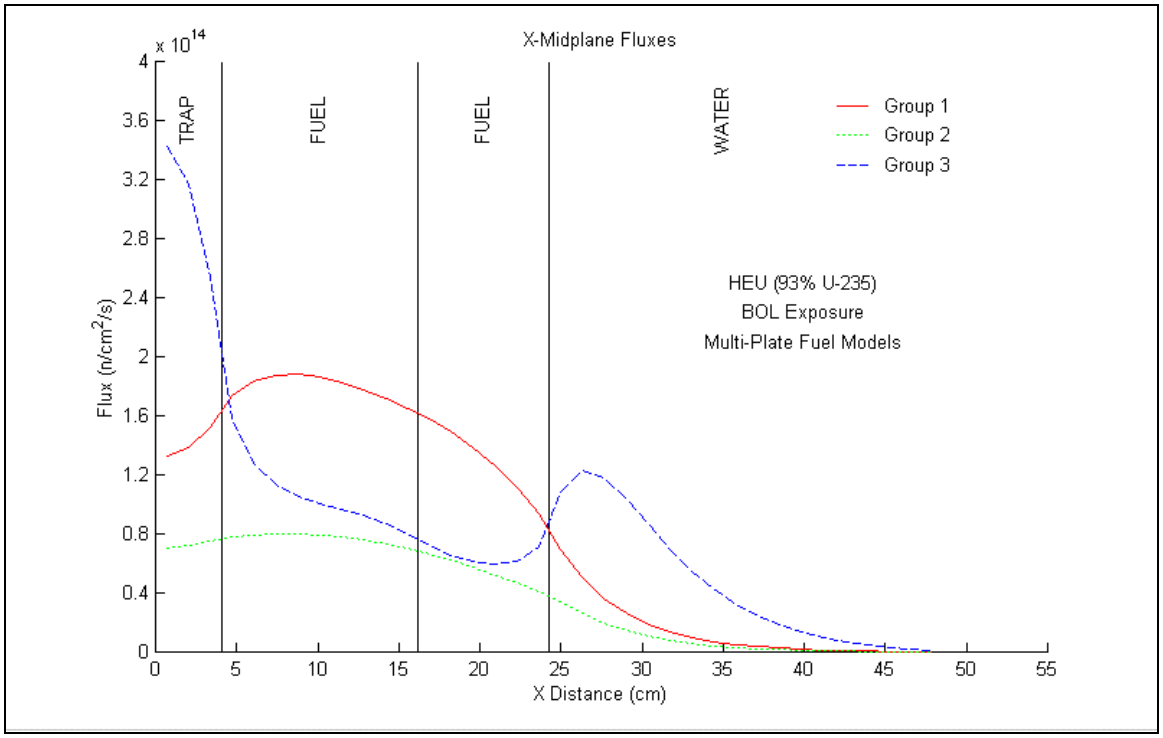

(b)

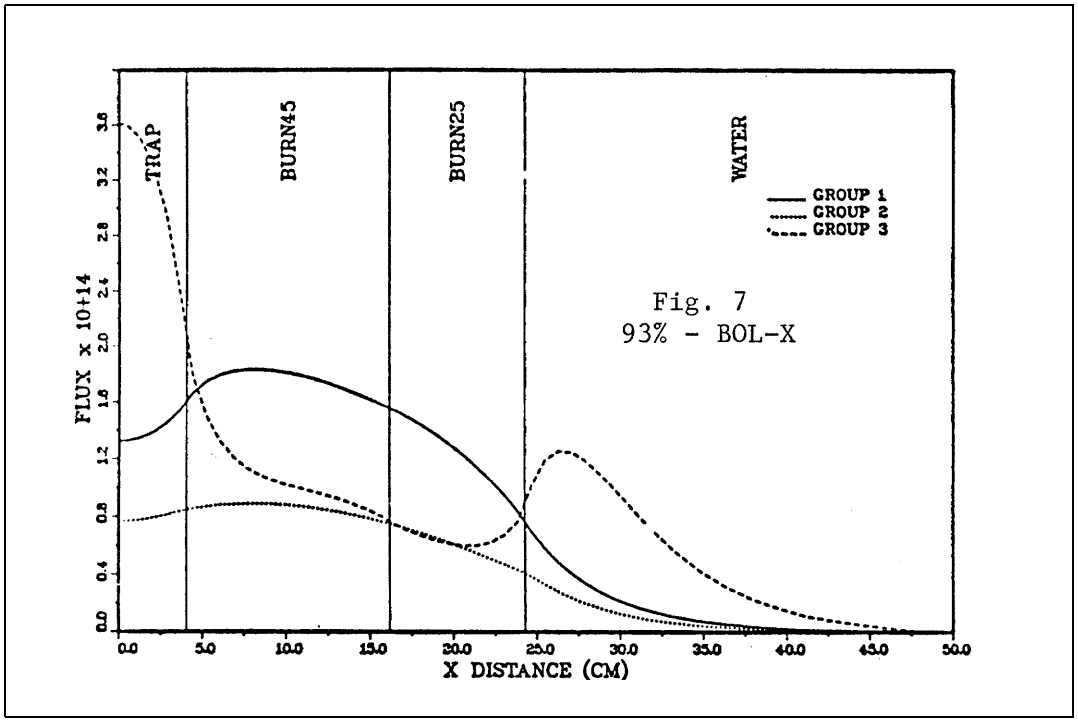

Figure 11: 93% Enrichment Core Midplane Fluxes at BOL Exposure Along the X-Axis (a) DRAGON/DONJON Results (b) ANL Results (Reproduced from Reference 1, Appendix F-1).

(a)

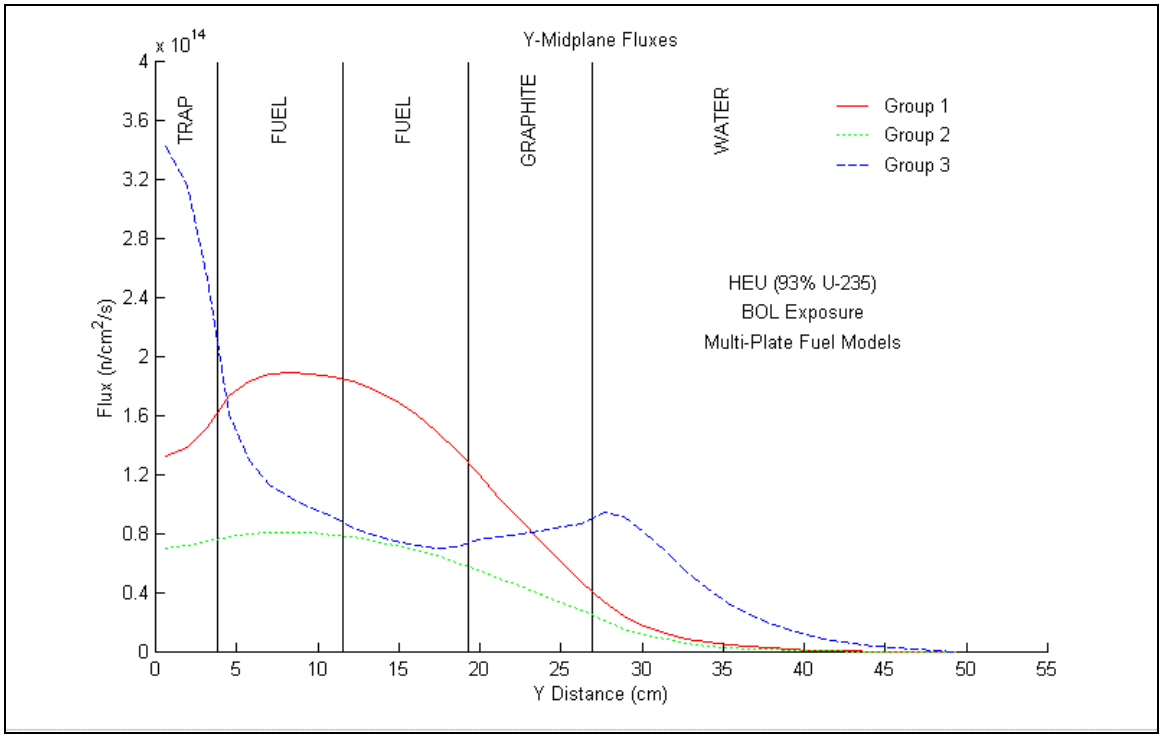

(b)

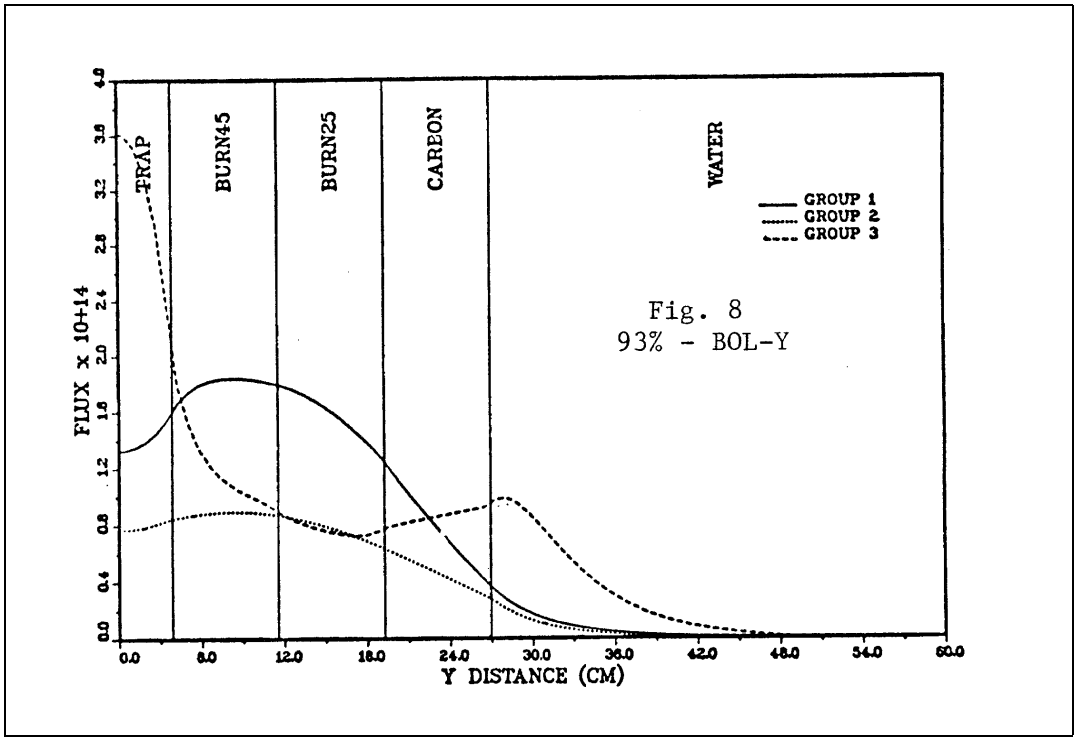

Figure 12: 93% Enrichment Core Midplane Fluxes at BOL Exposure Along the Y-Axis (a) DRAGON/DONJON Results (b) ANL Results (Reproduced from Reference 1, Appendix F-1).

(a)

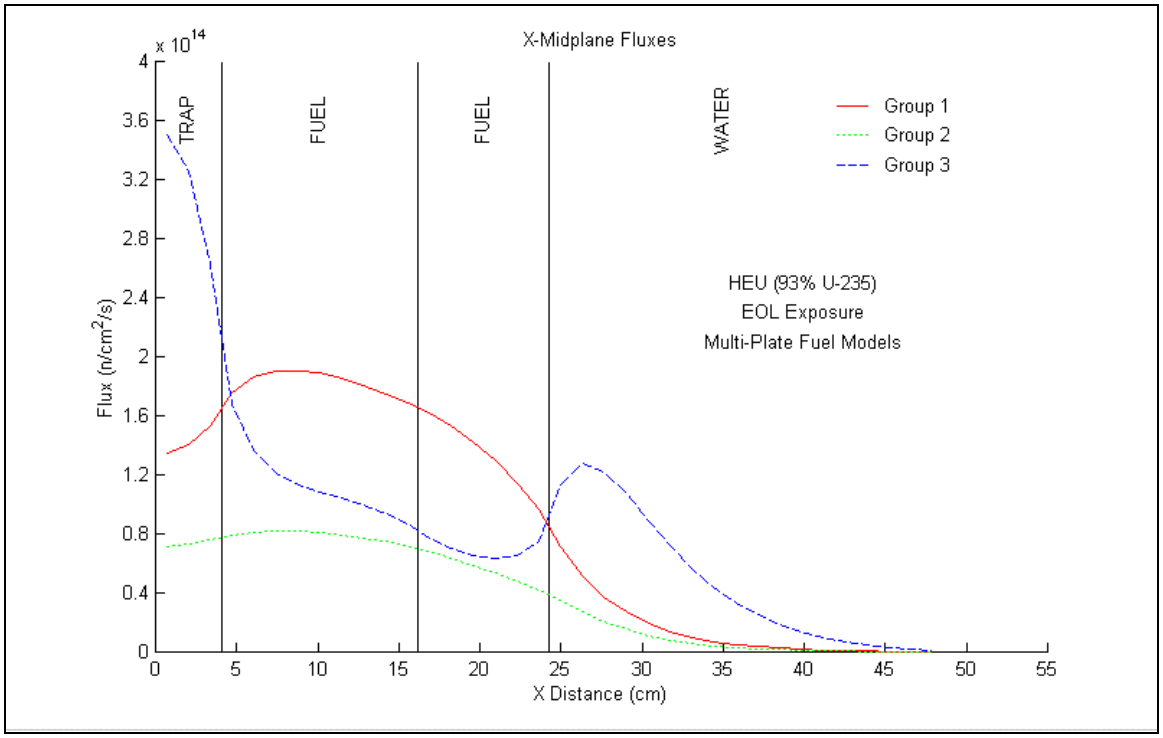

(b)

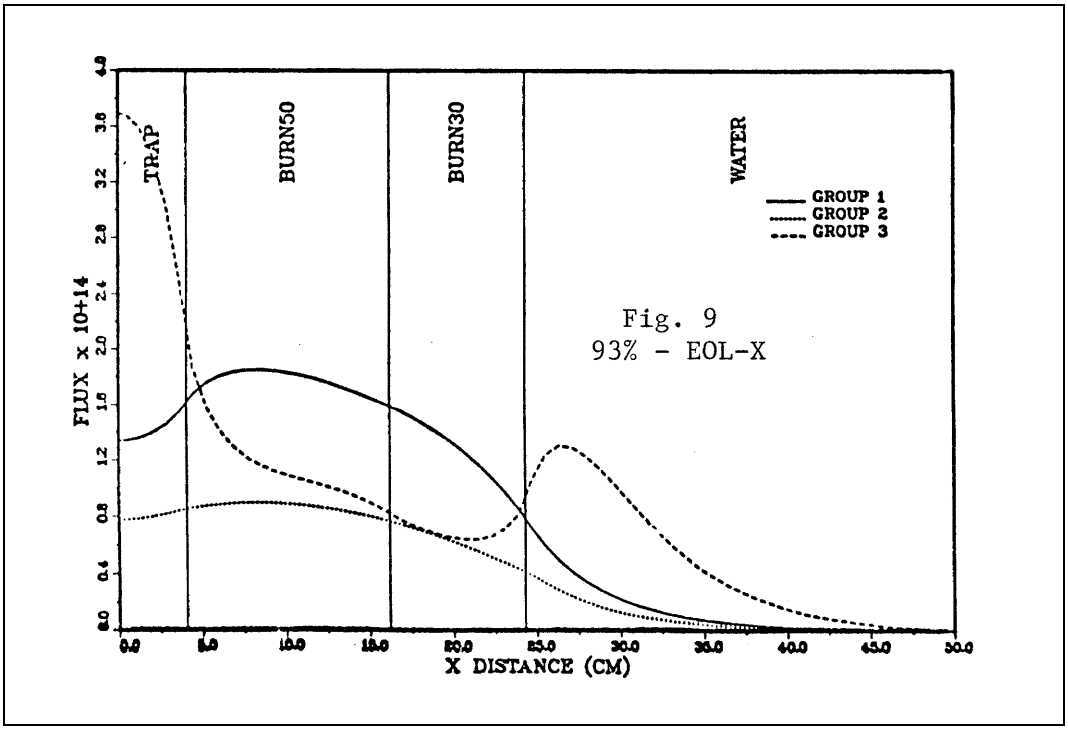

Figure 13: 93% Enrichment Core Midplane Fluxes at EOL Exposure Along the X-Axis (a) DRAGON/DONJON Results (b) ANL Results (Reproduced from Reference 1, Appendix F-1).

(a)

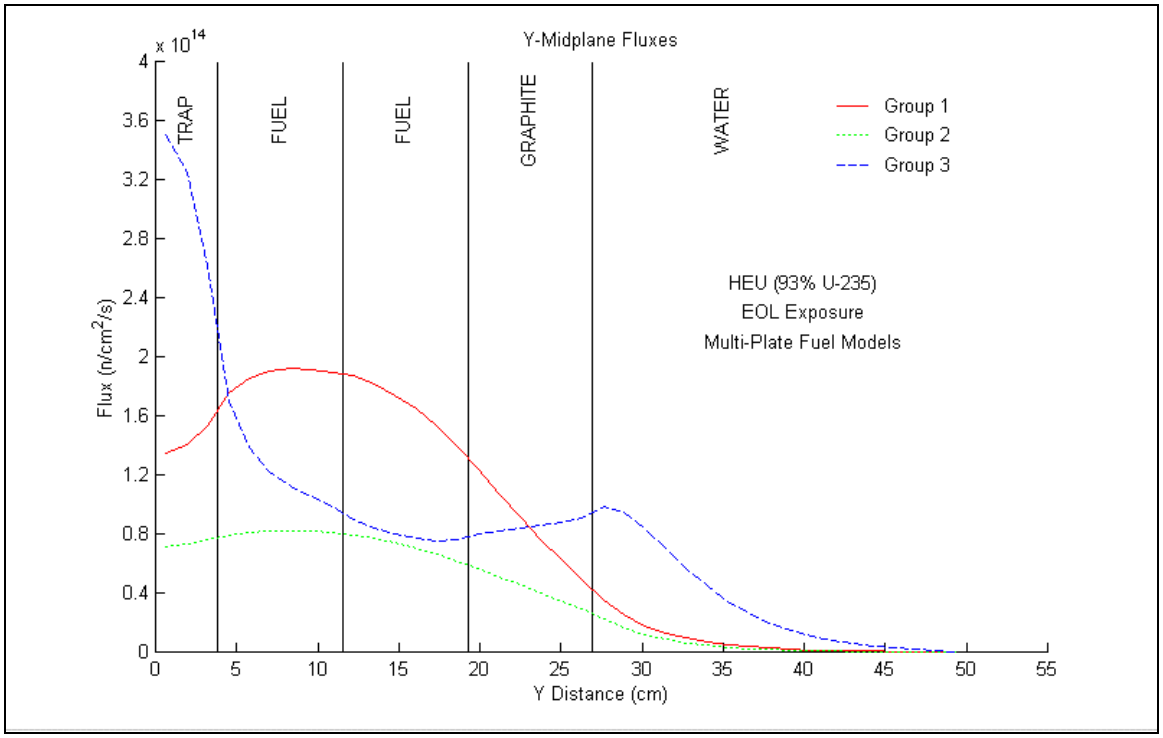

(b)

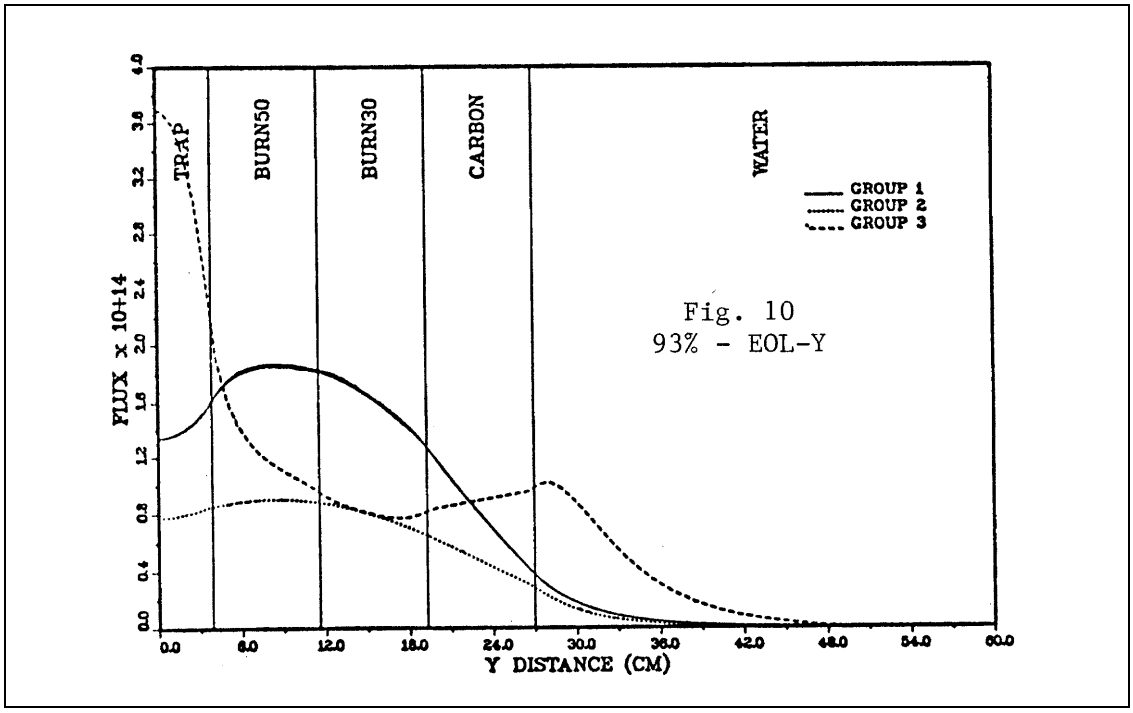

Figure 14: 93% Enrichment Core Midplane Fluxes at EOL Exposure Along the Y-Axis (a) DRAGON/DONJON Results (b) ANL Results (Reproduced from Reference 1, Appendix F-1).

(a)

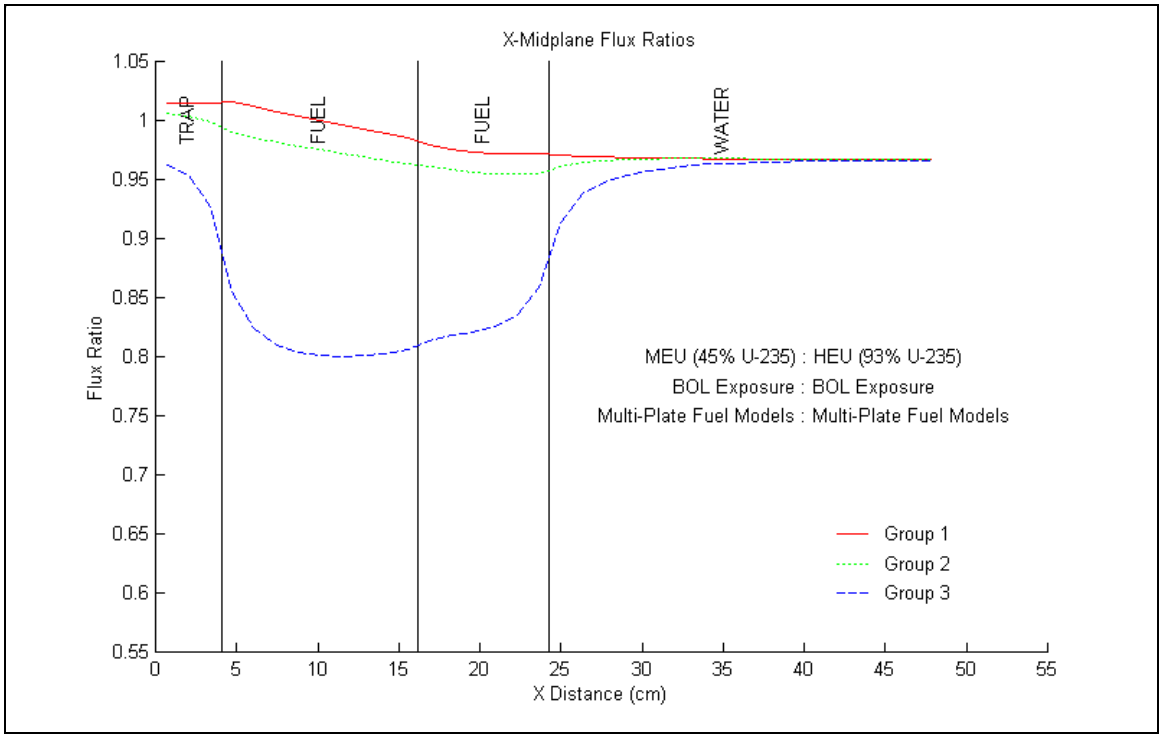

(b)

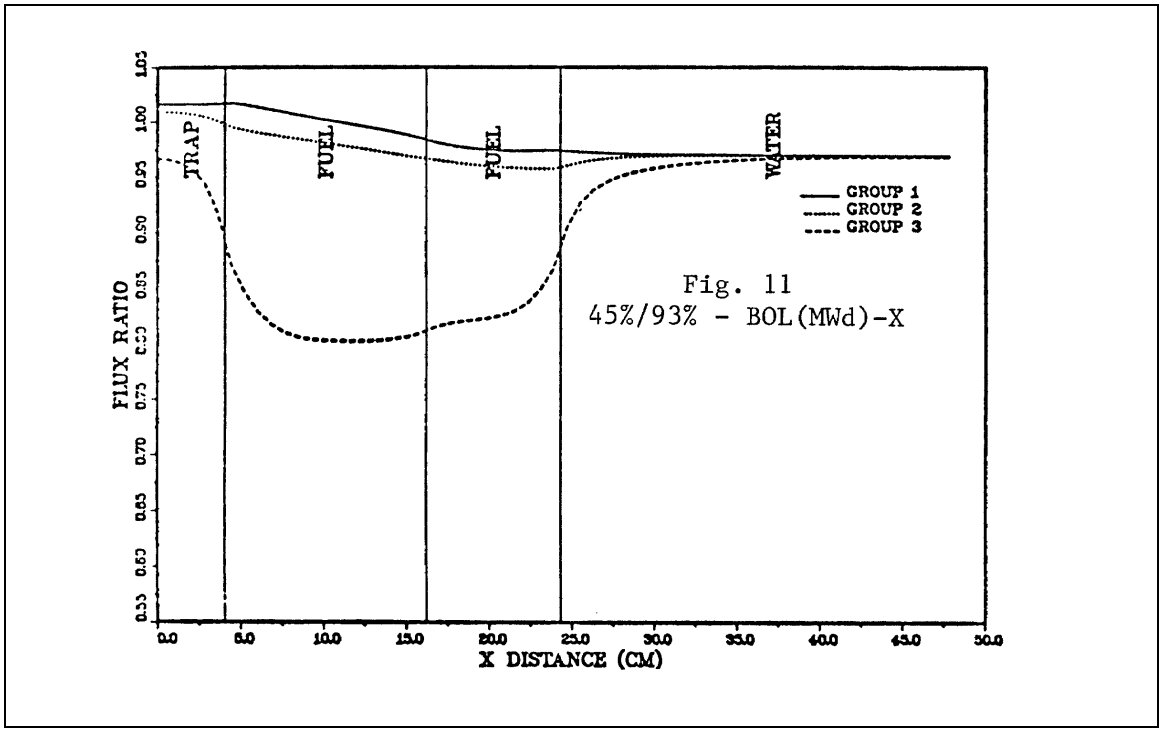

Figure 15: 45%/93% Enrichment Midplane Flux Ratios at BOL (Equal MWd) Exposure Along the X-Axis (a) DRAGON/DONJON Results (b) ANL Results (Reproduced from Reference 1, Appendix F-1).

(a)

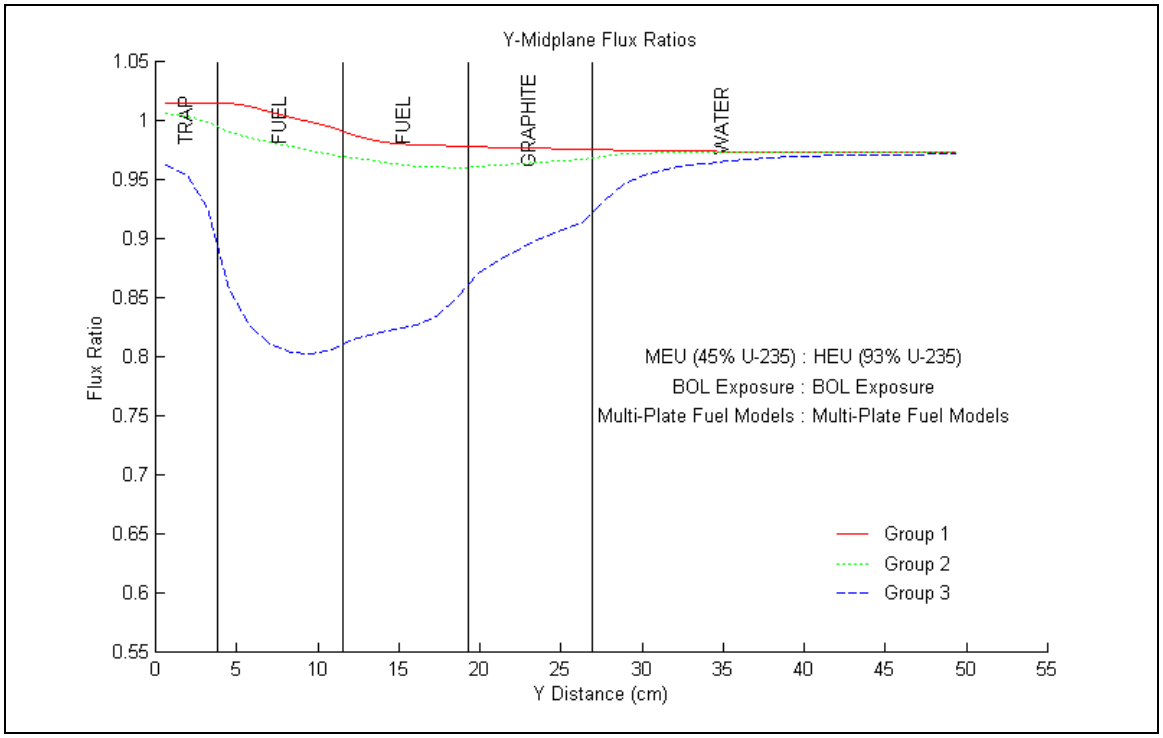

(b)

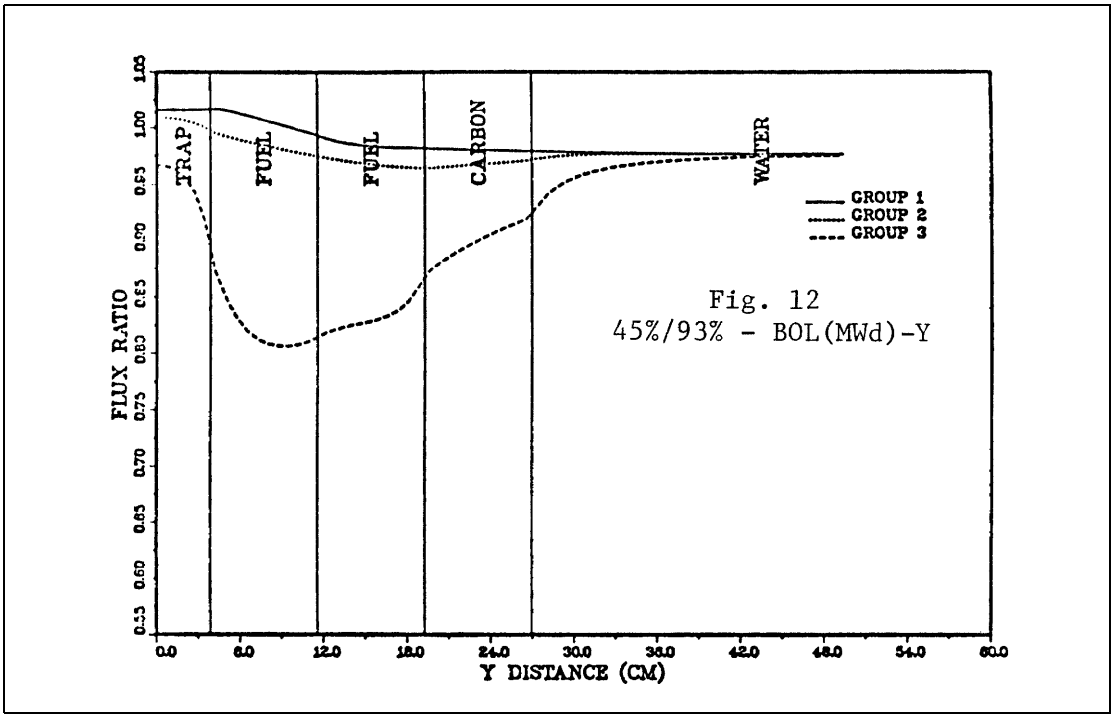

Figure 16: 45%/93% Enrichment Midplane Flux Ratios at BOL Exposure (Equal MWd) Along the Y-Axis (a) DRAGON/DONJON Results (b) ANL Results (Reproduced from Reference 1, Appendix F-1).

(a)

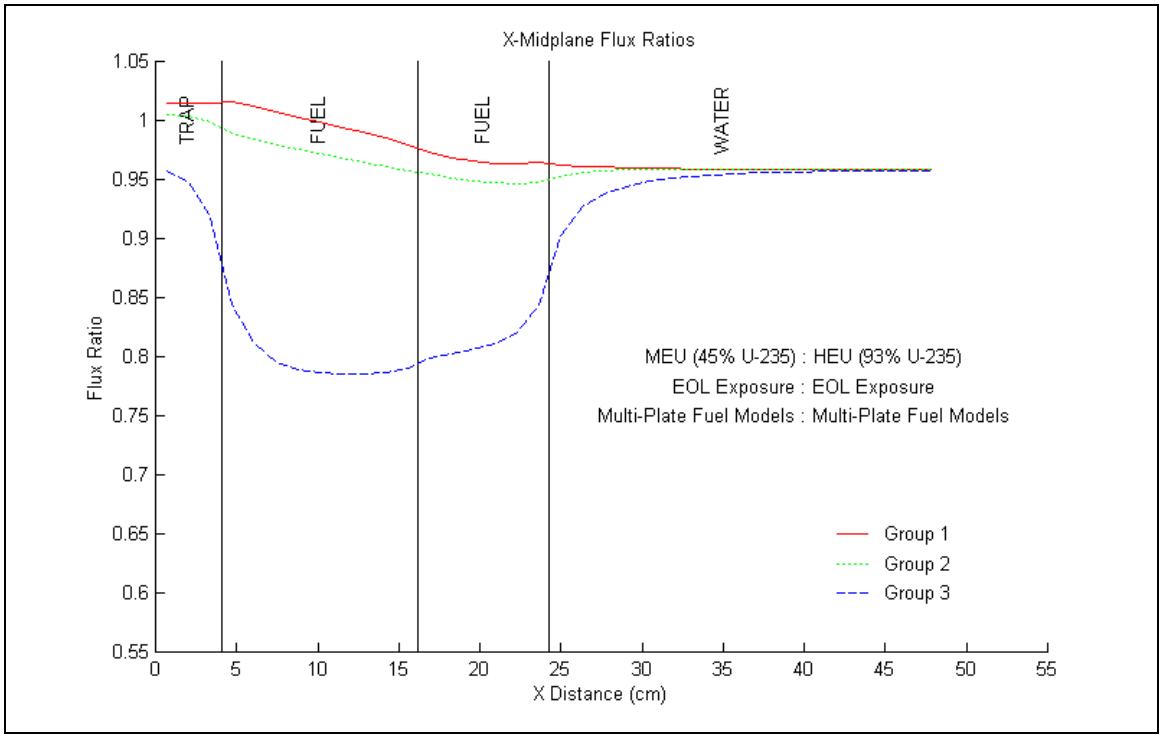

(b)

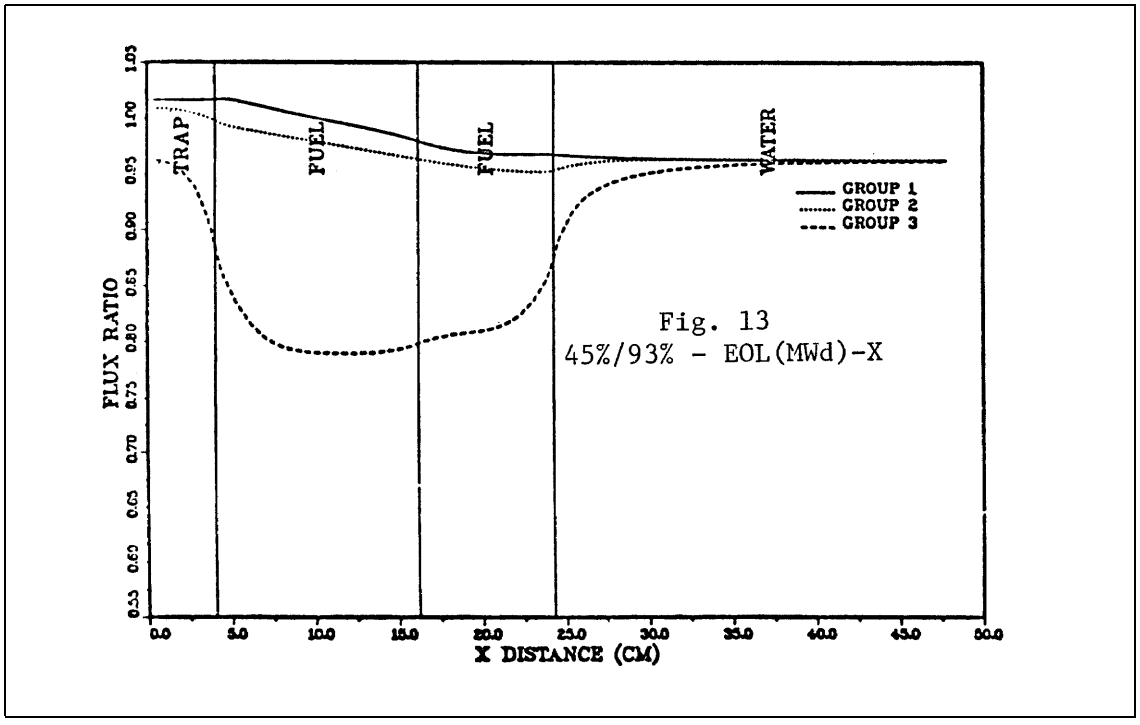

Figure 17: 45%/93% Enrichment Midplane Flux Ratios at EOL Exposure (Equal MWd) Along the X-Axis (a) DRAGON/DONJON Results (b) ANL Results (Reproduced from Reference 1, Appendix F-1).

(a)

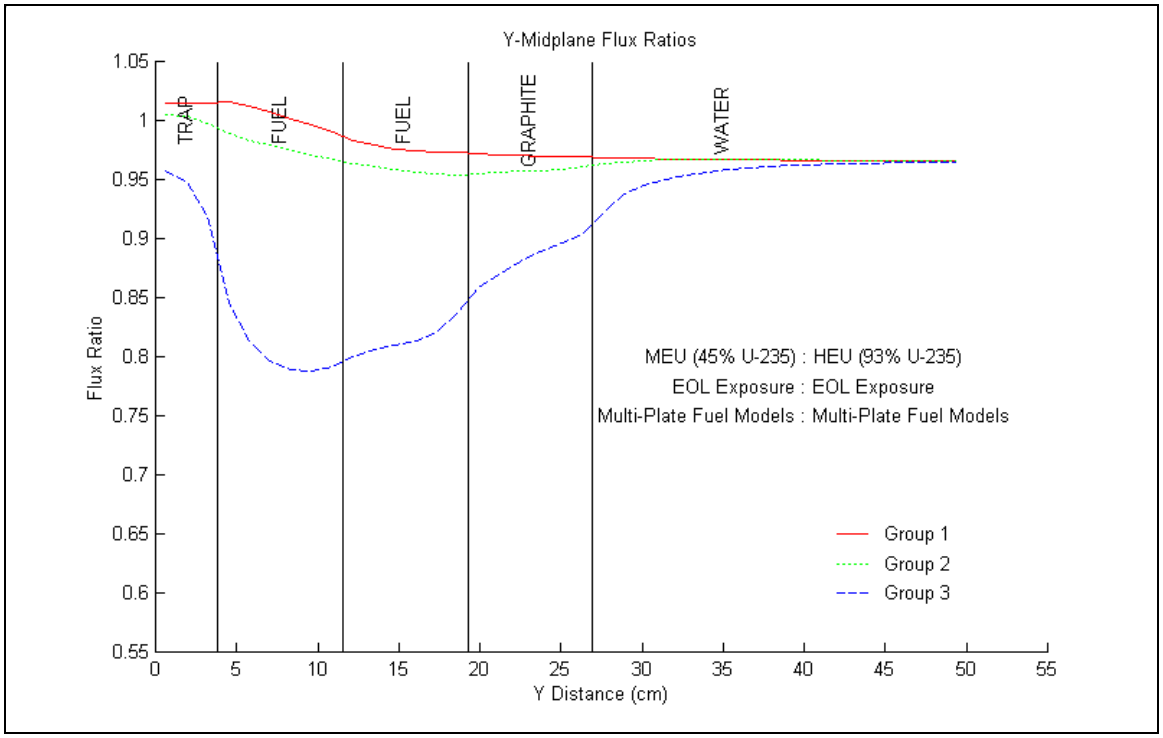

(b)

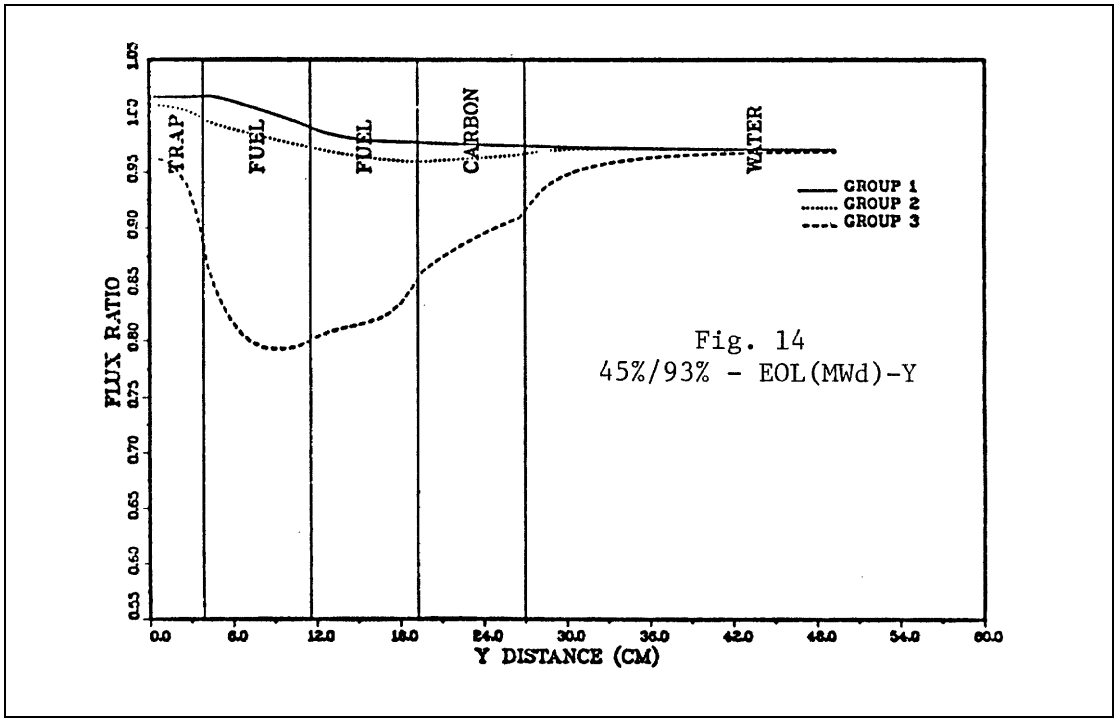

Figure 18: 45%/93% Enrichment Midplane Flux Ratios at EOL Exposure (Equal MWd) Along the Y-Axis (a) DRAGON/DONJON Results (b) ANL Results (Reproduced from Reference 1, Appendix F-1).

(a)

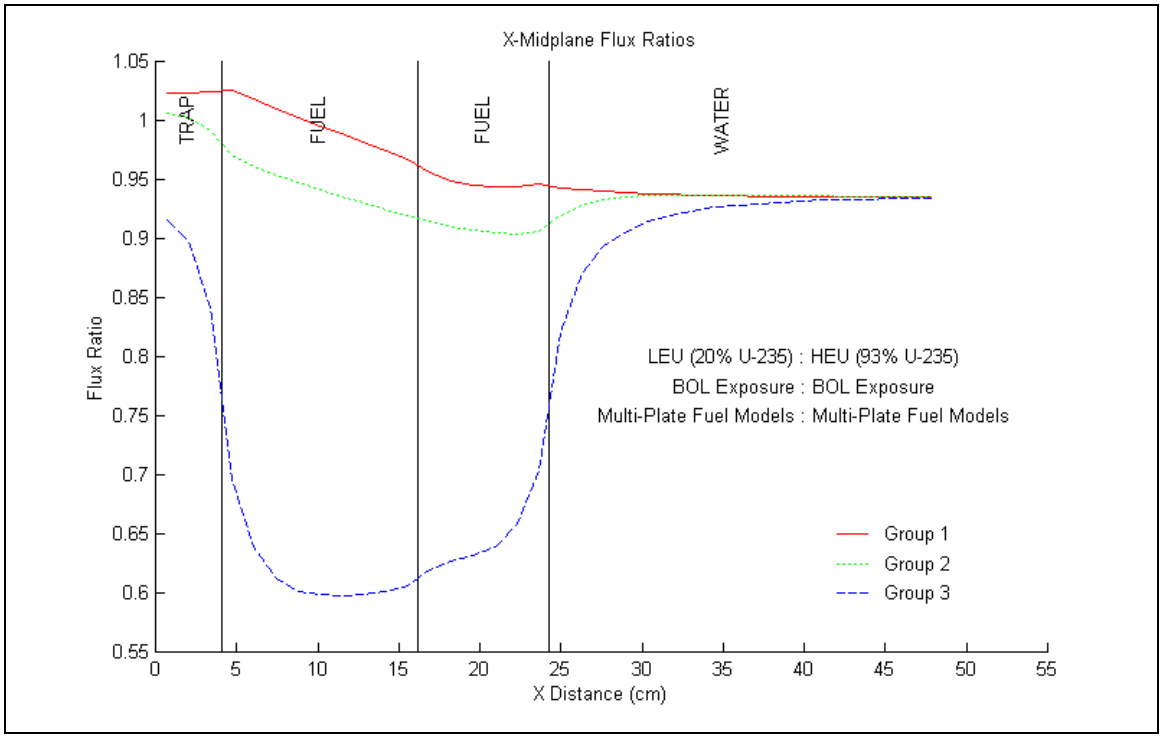

(b)

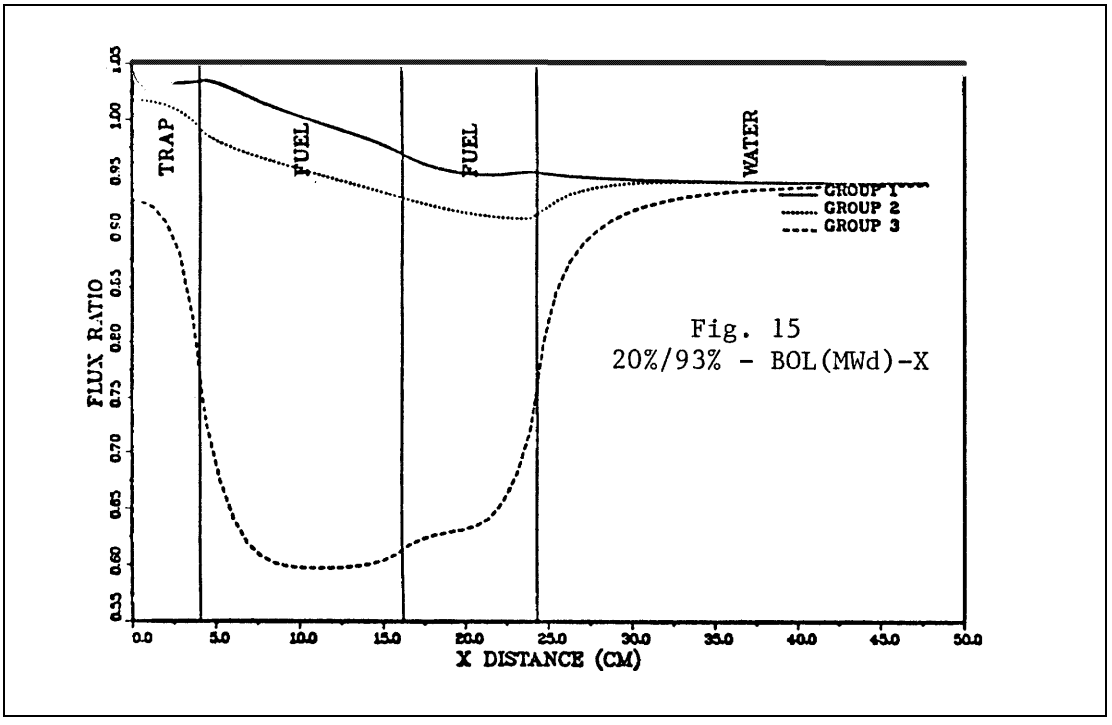

Figure 19: 20%/93% Enrichment Midplane Flux Ratios at BOL Exposure (Equal MWd) Along the X-Axis (a) DRAGON/DONJON Results (b) ANL Results (Reproduced from Reference 1, Appendix F-1).

(a)

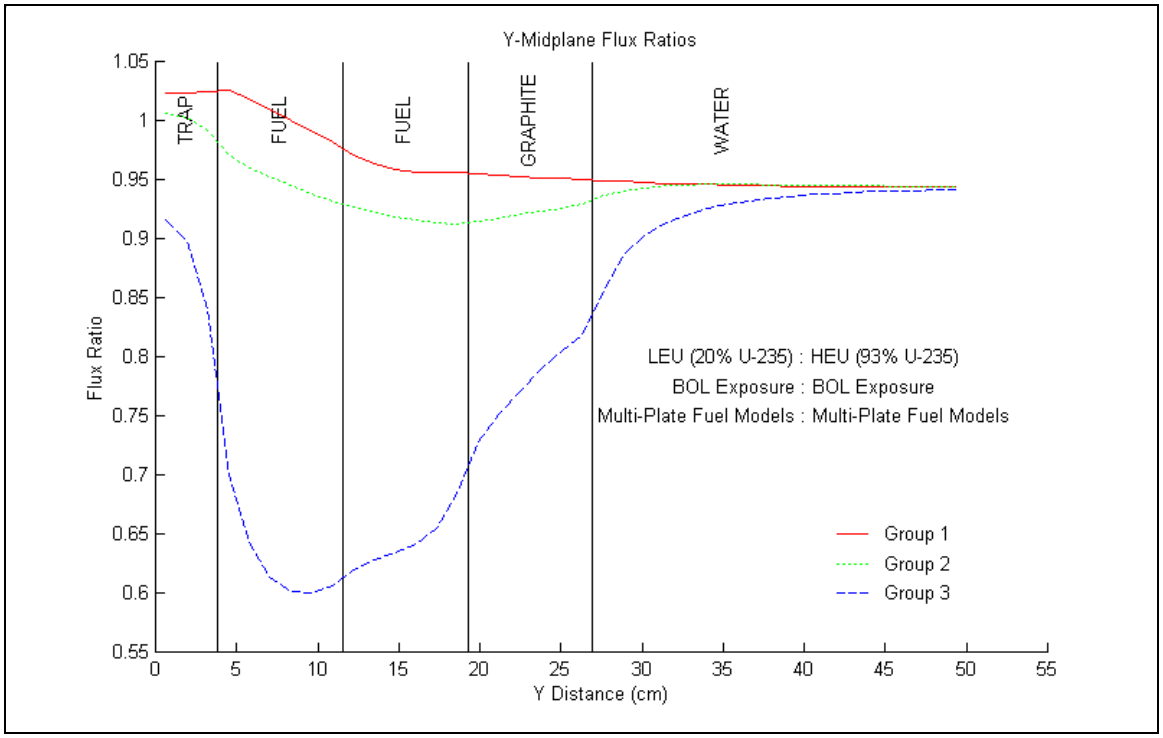

(b)

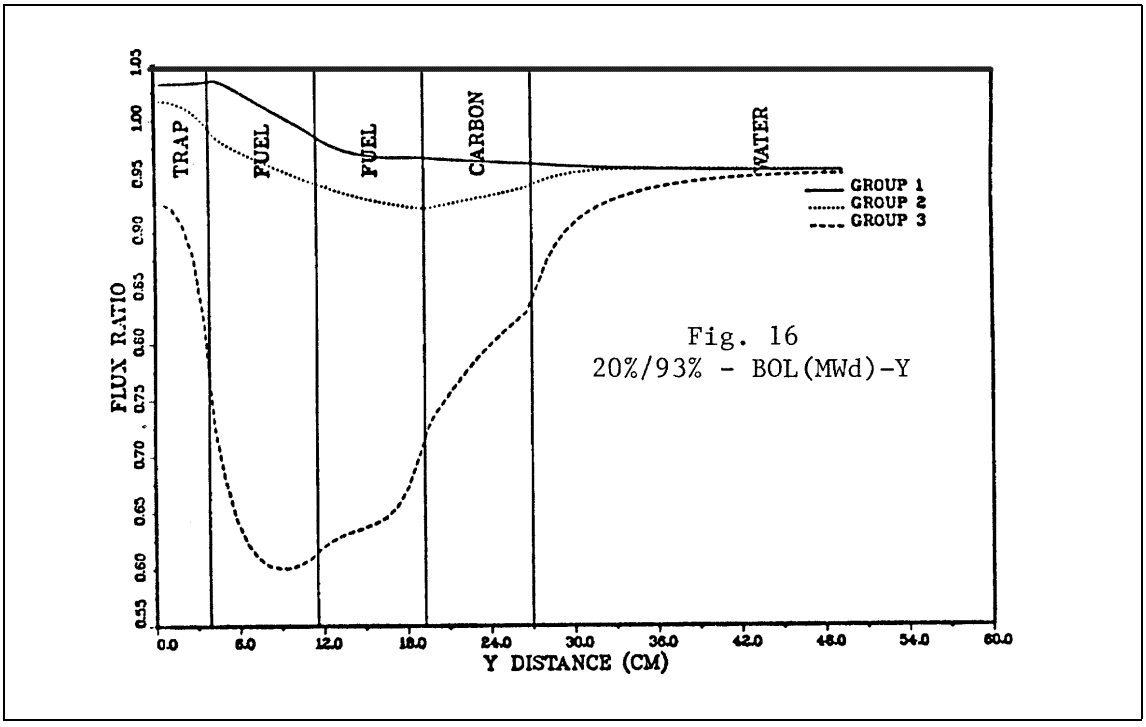

Figure 20: 20%/93% Enrichment Midplane Flux Ratios at BOL Exposure (Equal MWd) Along the Y-Axis (a) DRAGON/DONJON Results (b) ANL Results (Reproduced from Reference 1, Appendix F-1).

(a)

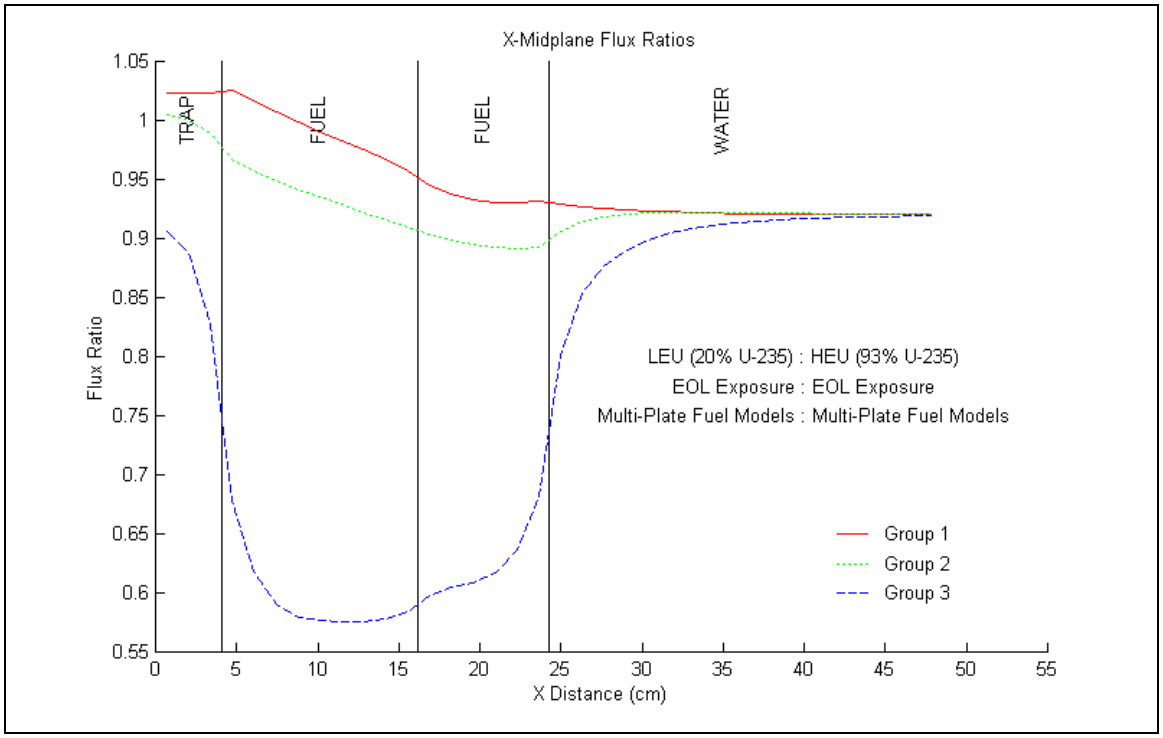

(b)

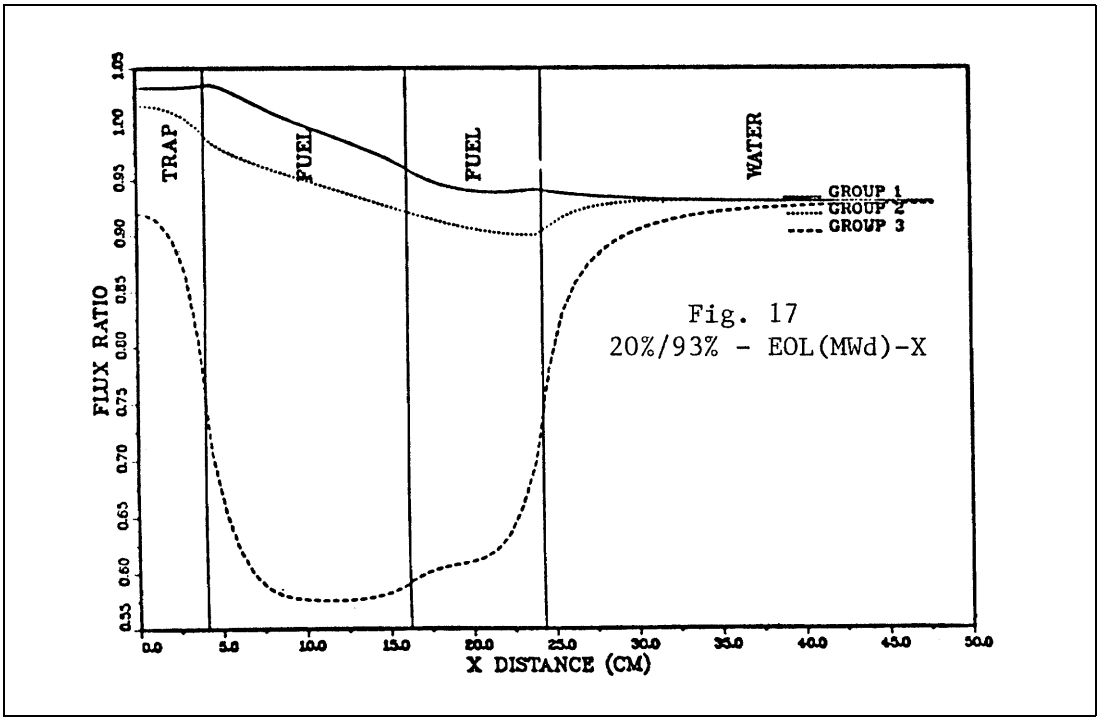

Figure 21: 20%/93% Enrichment Midplane Flux Ratios at EOL Exposure (Equal MWd) Along the X-Axis (a) DRAGON/DONJON Results (b) ANL Results (Reproduced from Reference 1, Appendix F-1).

(a)

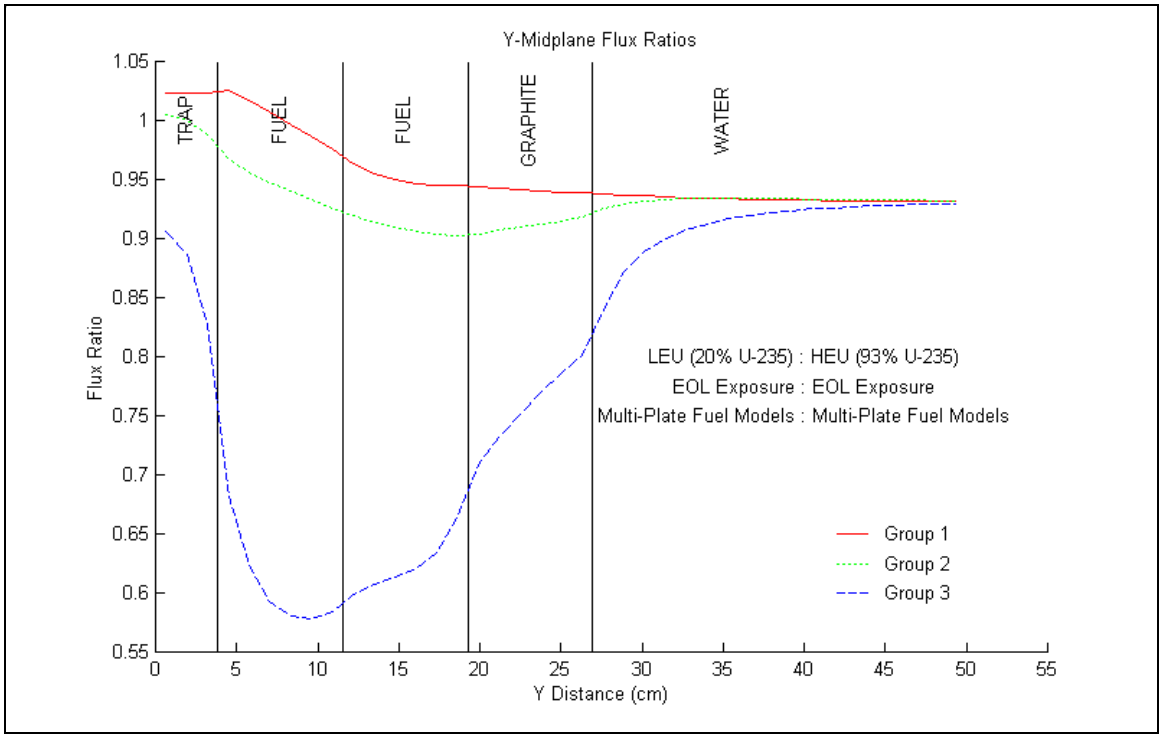

(b)

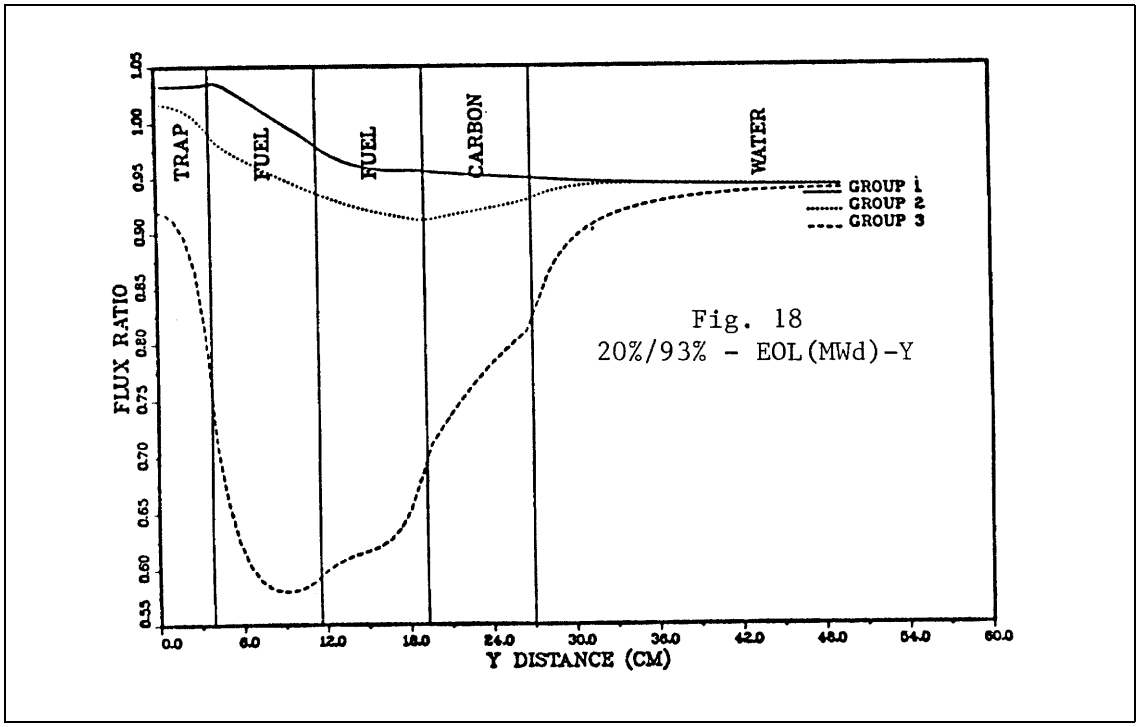

Figure 22: 20%/93% Enrichment Midplane Flux Ratios at EOL Exposure (Equal MWd) Along the Y-Axis (a) DRAGON/DONJON Results (b) ANL Results (Reproduced from Reference 1, Appendix F-1).